

UNIVERSITY OF CALGARY

Discerning Alveolar Macrophage Ontogeny in Mice

by

Wen Xuan Zhang

A THESIS

SUBMITTED TO THE FACULTY OF GRADUATE STUDIES
IN PARTIAL FULFILMENT OF THE REQUIREMENTS FOR THE
DEGREE OF MASTER OF SCIENCE

GRADUATE PROGRAM IN IMMUNOLOGY

CALGARY, ALBERTA

JUNE, 2023

©Wen Xuan Zhang 2023

Abstract

The adaptive and innate immunity are the two branches of the immune system our body uses to defend against invading microbes. After each encounter with a pathogen, the adaptive immune system develops a memory to prevent an infection with the same microbe. This ability to remember has recently also been shown in the innate immune system and was termed “trained immunity”, describing the ability to generate a stronger response towards a broad range of pathogens despite infection with just a single pathogen. The lung is an organ directly exposed to the microbes in the outside world, making it a likely site for immune cells to develop trained immunity. The predominant innate immune cells that reside in the lungs are the alveolar macrophages. These cells encounter countless pathogens every day and therefore are a likely cell in which to study trained immunity. Our lab recently figured out how to watch the macrophages crawl inside the lungs of living animals and this study examined how these macrophages behaved under different conditions (Neupane et al, 2020). However, these macrophages only live for a few months, so cells from the bone marrow constantly replace the macrophages, meaning that there are always two types of macrophages present in the lung. However, without an effective labelling tool, it was previously impossible to distinguish between the two macrophage populations, making their differences in behavior and function unknown. This study utilized a unique model to look at the two different macrophages and visualize these cells inside a living mouse to look for behavioural similarities and differences. Our findings determined the behavioral and functional similarities of these macrophages at homeostasis, their responses against the influenza virus, and provided support for both populations to be trained against influenza.

Preface

This thesis is original, unpublished, independent work by the author, W. Zhang. The experiments reported in Chapters 2-4 involving any animal use were reported and covered by the Animal Care Committee Approval Certification AC20-0121, issued by the University of Calgary Health Sciences ACC for the project “Discerning Alveolar Macrophage Ontogeny in Mice” on November 27, 2020.

Acknowledgements

As I complete my Master of Science degree, I recognize that my experience over the past three years has been a challenging, yet an incredibly enriching period of my life. This project would not have reached this stage with my efforts alone, and I would like to acknowledge the individuals that have played instrumental roles in bringing me to where I am today.

First and foremost, I would like to acknowledge my supervisor, Dr. Paul Kubes, for his support and patience since day one. He has played an incredible role in not only helping me grow as a student, but also as a researcher. He has spent countless hours teaching me, step by step, to deliver an excellent research presentation, write a scientific paper, review literature, analyze experiment data, and so much more. Thanks to him, I have grown to stand on my own and develop the skillsets to take ownership of my project. It is with sincere honor to have him as a mentor and recognize him as one of the biggest role models of my life.

Next, I would like to thank and acknowledge my supervisory committee Dr. Craig Jenne, and Dr. Margaret Kelly who have been important in helping me push my project forward. I would like to thank them for their questions which have helped me reflect on my project, critically appraise my research findings, and develop strategies to answer questions.

I would also like to acknowledge my two post-doctoral fellow mentors who have assisted me throughout my degree: Dr. Arpan Neupane and Dr. Fernanda Castanheira. Dr. Neupane has assisted me greatly in the beginning stages of my degree. He is hugely responsible for setting me on the right foot and helping me transition from an undergraduate student into a graduate student

researcher. My growth during my first year of my degree owe largely to him. Dr. Castanheira has been a fantastic mentor who has helped me on countless occasions with my experiments. She has heard my presentations the most times out of everyone in the lab and I am incredibly grateful for her willingness to keep providing feedback and her amazing assistance throughout my degree.

My development as a researcher also owes largely in part to the support from the post-doctoral fellows in Dr. Paul Kubes' lab. I would like to acknowledge my post-doctoral fellow colleague, Dr. Wanhai Qin, who has offered his expertise to help me understand the intricacies of epigenetics and lung immunology. I would like to thank him for his input in recognizing experiment limitations, teaching me how to extract information from literature, and helping me find all papers that I cannot find with his huge database. I would also like to extend my thanks to post-doctoral fellows Dr. Raymond Shim, for his gentle guidance and accompanying me on all the bubble tea trips, Dr. Marie Siwicki and Dr. Ysbrand Nusse, for their feedbacks on my scholarship applications, and Dr. Bruna David, for her kindness and warmth.

I would also like to acknowledge our lab technician, Michelle Willson, for helping me gain confidence in animal handling and teaching me my first intravital imaging surgery prep. She is responsible for helping me transition from enacting a fight-or-flight response to mice to being able to scruff a mouse under 15 seconds. My project would not be possible without the help from Trecia Nussbaumer, who has never failed to provide the mice that I need for my experiments first thing in the morning. I would like to thank Lori Zbytnuik in helping me with funding inquiries, organizing schedule conflicts with the lab, and managing my general inquiries. I would also like to acknowledge Dr. Woo Young Lee, for going so much above and beyond and making

those unnecessary trips to the lab on the weekend just to help me with microscope difficulties. Of course, I would also like to acknowledge Karen Poon, who has always been available to respond to my troubles with maneuvering the BD FACSCanto machine.

My time in the lab would not have been as entertaining and enjoyable without my lab mates. Josefien Hommes, who has been always available to chat and occasionally, share her wisdom about life. Oscar Tejada, who has been a pal and one of the few to enjoy my reckless driving. Rachita Panda, for her wonderful humor and uplifting advice. I would also like to acknowledge my fellow graduate colleagues: Nicole Sarden, who has been a close friend since my first day as a graduate student in MDSC 639.04. She has provided me with numerous help with managing graduate life, and for introducing me to the Immunology Graduate Association (IGA). I would like to thank Michelle Chen, for her help in editing my writing and listening to my practice presentations, and Emily Niu, for being beside me throughout my degree. I could always count on them for an evening pho night after a long and stressful day. Of course, I would also like to acknowledge my boyfriend, James Chen, who I have had the fortune to meet and share my hobbies with. I could always count on him to help me change gears and enjoy life outside of academia. Thank you for all the ski trips, badminton trips, jam sessions, and classical music concert nights – I could not ask for a better piano accompanist.

Lastly, I would like to extend my sincere thanks to my parents, Zhengfeng Cao, and Weiping Zhang, for their endless love and support over the years. My younger sister, Jenny Zhang, who has been a joy in the house and provided me with inspirational make-up advice, and of course, my lovely Ollie who has consistently been the first to greet me home.

Table of Contents

<i>Abstract</i>	<i>ii</i>
<i>Preface</i>	<i>iii</i>
<i>Acknowledgements</i>	<i>iv</i>
<i>List of Figures</i>	<i>ix</i>
<i>List of Symbols, Abbreviations, and Nomenclature</i>	<i>x</i>
Chapter One: Introduction and Literature Review	1
1.1 Introduction	1
1.2 Alveolar macrophages	3
1.2.1 Origin.....	3
1.2.2 AM behavior	4
1.2.3 Immune surveillance: Keeping the alveoli in check.....	6
1.3 Self-replenishment of tissue-resident macrophages	12
1.3.1 Self-replenishment of TR-AMs through local proliferation.....	12
1.4 Monocyte-derived Alveolar Macrophages (MO-AMs)	13
1.4.1 Origin: Monocytes	13
1.4.2 Recruitment of monocytes into tissues during infection.....	17
1.4.3 Replenishing TR-AMs with MO-AMs during inflammation.....	18
1.4.4 Turnover of tissue-resident macrophages with age	19
1.4.5 Monocytes can perform the homeostatic roles of resident macrophages.....	20
1.5 TR-AMs vs. MO-AMs	21
1.5.1 AM markers	21
1.5.2 The roles of TR-AMs and MO-AMs at homeostasis.....	21
1.5.3 TR-AMs and MO-AMs during respiratory infections.....	22
1.6 Trained immunity	23
1.6.1 The emergence of innate immune memory.....	23
1.6.2 Epigenetic modification.....	24
1.6.3 β -glucan as a trained immunity tool.....	25
1.6.4 Training alveolar macrophages.....	26
1.7 Rationale	27
1.8 Hypothesis and Specific Aims	28
Chapter Two: Materials and Methods	29
2.1 Animals	29
2.2 <i>In vivo</i> labelling of AMs	29
2.3 Oropharyngeal administration of reagents	30
2.4 Preparation of the lung for imaging and IVM	30
2.5 <i>In vivo</i> depletion of AMs	31
2.6 Collecting the bronchoalveolar lavage fluid (BALF)	32

2.7	Flow Cytometry (FACs) preparation	32
2.8	Plaque Forming Unit (PFU) assay.....	33
2.9	IAV infection	35
2.10	<i>S. aureus</i> growth and infection in mice	35
2.11	β -glucan administration	36
2.12	Experimental protocol for comparing TR-AMs and MO-AMs at homeostasis	36
2.13	Statistical analysis	37
Chapter 3. The Turnover and Behavior of TR-AMs and MO-AMs at homeostasis		38
3.1	Results	38
3.1.1	Turnover of TR-AMs to MO-AMs increase with age.....	38
3.1.2	Similar net displacement of TR-AMs and MO-AMs at homeostasis at 8-weeks.....	43
3.1.3	Phagocytic ability of TR-AMs and MO-AMs are similar at homeostasis.....	46
3.1.4	TR-AMs renew with minimal contribution from MO-AMs following clodronate-liposome-induced depletion	50
3.1.5	BAL Turbidity before and 14 days after clodronate administration is not significantly different 53	
3.1.6	Phagocytic ability of TR-AMs and MO-AMs remain the same post-CLL depletion.....	55
3.2	Discussion	58
Chapter 4. Training TR-AMs and MO-AMs against IAV infection		65
4.1	Results	65
4.1.1	TR-AMs and MO-AMs are both paralyzed after IAV infection	65
4.1.2	β -glucan-induced inflammation resolves 14 days post-administration	70
4.1.3	No turnover of TR-AMs to MO-AMs 14 days .after β -glucan treatment	74
4.1.5	β -glucan does not alter CD11b ⁺ expression in AMs post-IAV infection.....	78
4.1.6	TR-AM and MO-AM paralysis post-IAV infection have both been restored with prior treatment with β -glucan.	80
4.2	Discussion	82
Chapter 5. Limitations and future directions.....		85
5.1.	Limitations and future directions	85
5.2.	Summary.....	88
References.....		90
Appendix A.....		102
Table 1. List of antibodies used		102
Table 2. List of bacteria and virus used.....		102
Table 2. List of chemicals, peptides, and reagents used.....		102
Table 4. List of software used		103

List of Figures

Figure 1.1. AM migrate across alveoli and engulf foreign particles and clean the alveolar space.	6
Figure 1.2. Monocyte development, recruitment, and differentiation into tissue-resident macrophages.	16
Figure 3. 1. Percentage of MO-AMs increase in the AM population increase with advancing age.	41
Figure 3. 2. TR-AM to MO-AM turnover increase with advancing age from 8- to 40- weeks.	42
Figure 3. 3. Net displacement of TR-AMs and MO-AMs is similar in 8-week mice but different in 40-week mice.	45
Figure 3. 4. 4×10^6 CFU of <i>S. aureus</i> bacteria is the maximum infection dose that avoids a lung inflammatory response.	48
Figure 3. 5. Phagocytic ability of TR-AMs and MO-AMs is similar at 8 and 16-weeks.	49
Figure 3. 6. Alveolar macrophage numbers recover 60% by 14 days post-CLL treatment and are predominantly TR-AMs.	51
Figure 3. 7. Optical density 600 (OD600) (turbidity) of BAL supernatant remains similar at 14 days after clodronate liposome treatment.	54
Figure 3. 8. Percentage of TR-AMs and MO-AMs with bacteria remain the same. CFU and neutrophil number in the BAL after <i>S. aureus</i> infection after clodronate liposome treatment.	56
Figure 4. 1. TR-AMs and MO-AMs are both paralyzed at 12 days post-IAV infection in 8- and 40-week mice.	67
Figure 4. 2. TR-AMs and MO-AMs are similarly paralyzed at 8-weeks but different at 40-weeks after 12 days post-IAV.	69
Figure 4. 3. Neutrophils, eosinophils and monocytes in the lung increase at 5 days and drops at 14 days post-β-glucan administration but total AM number remains the same.	72
Figure 4. 4. No turnover of TR-AM to MO-AM at 14 days post β-glucan treatment.	75
Figure 4. 5. β-glucan treatment prevents the IAV-induced AM paralysis of AMs.	77
Figure 4. 6. Median Fluorescent Intensity (MFI) of CD11b is not different in AMs after IAV infection in PBS and β-glucan pre-treated conditions.	79
Figure 4. 7. The motility of TR-AMs and MO-AMs are restored at 12 days post-IAV infection after prior treatment with β-glucan.	81

List of Symbols, Abbreviations, and Nomenclature

ACK	Ammonium-chloride-potassium
AEC1	Alveolar epithelial type I cell
AEC2	Alveolar epithelial type II cell
AF	Auto-fluorescence
AM	Alveolar macrophage
BAL or BALF	Bronchoalveolar lavage fluid
BCG	Bacillus Calmette Guerin
BSA	Bovine serum albumin
C. albicans	Candida albicans
C57BL/6	C57 black 6 inbred laboratory wild-type mice
CCL2	CC-chemokine ligand 2
CCR2	C-C chemokine receptor 2
CFU	Colony forming units
CLL	Clodronate liposomes
CMoP	Common monocyte progenitor
CMP	Common myeloid progenitor
CX3CR1	C-X-C motif chemokine receptor-1
CXCL1, 2, 9	Chemokine ligand-1, -2, -9
DC	Dendritic cell
DMEM	Dulbecco's modified Eagle's medium
DTR	Diphtheria toxin receptor
E. coli	Escherichia coli
EDTA	Ethylenediaminetetraacetic acid
FACs	Fluorescence activated cell sorting or Flow cytometry
FOV	Field of view
FOXP3	Forkhead box P3
GFP	Green fluorescent protein
GM-CSF	Granulocyte-macrophage colony stimulating factor
GMP	Granulocyte-monocyte progenitors
H3K27ac	Histone 3 lysine 27 acetylation
H3K4me	Histone 3 lysine 4 trimethylation
HBSS	Hanks' balanced salt solution
HDM	House dust mite
HSC	Hematopoietic stem cells
HSPC	Hematopoietic stem and progenitor cells
IAV	Influenza A virus
IFN γ	Interferon gamma
IL-1, 6, 10	Interleukin-1, 6, 10
IP	Intraperitoneal
IT	Intratracheal
IVM	Intravital microscopy
KC	Keratinocyte-derived chemokine
KO	Knockout
LPS	Lipopolysaccharide

Ly6C	Lymphocyte antigen 6C
M-CSF	Macrophage colony-stimulating factor
M. tuberculosis	Mycobacterium tuberculosis
MARCO	Macrophage receptor with collagenous structure
MDCK	Madin-Darby Canine Kidney
MDP	Monocyte-DC progenitors
MIP-2	Macrophage inflammatory protein-2
MO-AM	Monocyte-derived alveolar macrophage
MPS	Mononuclear phagocyte system
MuHV-4	Murid herpesvirus 4
NADH	Nicotinamide adenine dinucleotide (NAD) + hydrogen (H)
OD	Optical density
P. aeruginosa	Pseudomonas aeruginosa
PAP	Pulmonary alveolar proteinosis
PBS	Phosphate buffered saline
PFA	Paraformaldehyde
PFU	Plaque forming units
PPAR- γ	Peroxisome proliferator-activated receptor gamma
RAG-1	Recombination activating gene-1
RBC	Red blood cell
RNA	Ribonucleic acid
ROS	Reactive oxygen species
ROS	Reactive oxygen species
RPMI	Roswell Park memorial institute
S. aureus	Staphylococcus aureus
S. pneumoniae	Streptococcus pneumoniae
scATAC	Single-cell assay for Transposase-Accessible Chromatin
SCID	Severe combined immunodeficient
scRNA	Single-cell RNA
SiglecF	Sialic acid-binding immunoglobulin-like lectin F
SOCS3	Suppressor of cytokine signaling-3
SPA	Surfactant protein A
SPD	Surfactant protein D
STAT	Signal transducer and activator of transcription
TCA	Tricarboxylic acid cycle
TdT	TdTomato
TGF β	Transforming growth factor β
TNF α	Tumor necrosis factor α
TPCK	N-tosyl-L-phenylalanine chloromethyl ketone
TR-AM	Tissue-resident alveolar macrophage
WT	Wild-type

Chapter One: Introduction and Literature Review

1.1 Introduction

The lungs are the largest organ in the human respiratory system and perform the vital function of gas exchange. Every day, 10,000 L of air enter the upper respiratory tract consisting of the nose and throat, and subsequently enter the trachea and alveoli. Oxygen and carbon dioxide exchange between the alveoli and blood vessel, serving as the most critical function of the lung.

At the terminal branch, the alveoli are lined with epithelial cells that optimize the structure of the alveoli to facilitate efficient gas exchange. There are two types of epithelial cells – type I and type II pneumocytes – which span the lining of the alveolar lumen. Type I pneumocytes cover 95% of the surface area and share a basement membrane with the capillary endothelium forming a very narrow interstitial space to perform gas exchange. Type II pneumocytes cover 5% of the alveoli and are a source of surfactant, decreasing the surface tension and preventing the alveoli from collapsing (Brandt et al, 2022; Ward et al, 1984). Finally, residing in the alveoli are the innate immune cells that are primarily responsible for responding to foreign particles and patrolling the alveolar spaces to maintain pulmonary homeostasis.

Alveolar macrophages (AMs) constitute over 90% of the immune cells in the alveoli (dendritic cells and lymphocytes occupy the remaining 10%) and proliferate in the alveoli throughout life. As smoke, dust, and other particulates enter the alveoli, AMs are responsible for recognizing and removing unwanted particles from the lung. This ability is the primary homeostatic role of AMs upon recognition of foreign particles and pathogens. However, since the air is replete with non-sterile particles that can stimulate a robust immune response, AMs also

incorporate several mechanisms to avoid unnecessary inflammatory responses that can damage the lung (Ginhoux et al, 2016; Epelman et al, 2014). AMs populate the lungs prior to birth and reside in the alveoli as tissue-resident alveolar macrophages (TR-AMs). Although TR-AMs were believed to maintain their numbers through self-renewal, recent studies suggest that TR-AMs are gradually replaced by monocyte-derived alveolar macrophages (MO-AMs) over time (Liu et al, 2019). However, due to technical limitations, TR-AMs and MO-AMs remain visually indistinguishable thus, making it impossible to differentiate their behaviors and functions.

As cells that are directly exposed to the outside world, AMs encounter many pathogens and perhaps learn to deal with these invaders. As a result, AMs have become potential candidates for the study of trained immunity, which describes memory formed by the innate immune system. Different from adaptive immune memory where adaptive immune cells developed increased responsiveness towards a specific pathogen, trained immunity suggests that innate immune cells can develop increased, but non-specific responsiveness towards many pathogens. Although increasing research has studied this concept in a number of cells including monocytes and macrophages, whether TR-AMs and MO-AMs can be trained remains unknown. This thesis will explore the behaviors and functions of TR-AMs and MO-AMs at homeostasis, compare their abilities to phagocytose bacteria, and their respective abilities to be trained.

1.2 Alveolar macrophages

1.2.1 Origin

Historically, AMs were classified as part of the mononuclear phagocyte system (MPS), and along with other tissue-resident macrophages such as Kupffer cells, microglia, and Langerhan cells, was thought to derive from circulating monocytes (van Furth and Cohn, 1968; Geissman et al, 2003; Geissman et al, 2010; Godleski and Brain, 1972). This idea was primarily supported by evidence of monocytes demonstrating the capability to differentiate into tissue-resident macrophages. For example, it has been shown that depletion of AMs by intratracheal (IT) administration diphtheria toxin in CD11c-DTR mice, followed by adoptive transfer of adult monocytes demonstrated that monocytes can differentiate into macrophages (Geissman et al, 2003; Landsman and Jung, 2007). Further, in a chimera model where mice were lethally irradiated, it was shown that transferred bone marrow cells subsequently divided into macrophages (Virolainen, 1968; van aud Ablas and van Furth, 1979). However, this theory has been challenged by opposing evidence. Using fate-mapping models such as the transgenic CX3CR1-Cre mouse model, Yona *et al.* showed that macrophages self-renew to replenish their population independently of monocytes (Yona et al, 2013). Further, it was suggested that tissue-resident macrophages appear in the embryonic tissues prior to the development of monocytes, challenging the concept that monocytes can serve as a precursor to macrophages (Takahashi et al, 1989; Ginhoux et al, 2010; Hoeffel et al, 2012; Schulz et al, 2012). Although undeniable that monocytes are capable of differentiating into macrophages, they are unlikely the origin of all pre-natal macrophages and may not replace macrophages in all tissues.

Yolk-sac and fetal liver progenitor cells have been identified as two sources of tissue-resident macrophages. Using fate-mapping tools, it was suggested that microglia and cardiac macrophages are derived from the yolk-sac that seed into the brain and heart respectively and proliferate locally at steady state with no input from circulating monocytes (Ginhoux et al, 2010). It was proposed that these yolk-sac cells colonized the individual tissues in the embryo and matured into self-renewing macrophages (Higashi et al, 1992; Takeya and Takahashi, 1992). Subsequently, Kupffer cells, peritoneal macrophages, Langerhans cells, splenic macrophages, and kidney macrophages were all proposed to derive independently from monocyte precursors, leading to the generalization that tissue-resident macrophages are yolk-sac and fetal liver-derived (Schulz et al, 2012, Yona et al, 2013). As for the lungs, Guillams *et al.* proposed in 2013 that AMs were derived from the fetal liver monocytes that seed into the lung prior to birth and develop into macrophages (Guillams et al, 2013). In addition, Evren *et al.* also demonstrated the fetal liver origin of human AMs in a humanized mouse model *in vivo* (Evren et al, 2021). It was identified that human AMs originate in the fetal liver that then migrate into the blood and then the lung, where they develop into AMs. The development and growth of AMs from fetal liver monocytes in the lung is critically regulated by GM-CSF, which is produced by the alveolar epithelial type 2 cells (AEC2) (Guillams et al, 2013).

1.2.2 AM behavior

Motility, described as the ability to displace over time, has been well noted as an important mechanism for the function of innate immune cells. For example, the classic neutrophil cascade incorporating adhesion, crawling, and transmigration is imperative for neutrophils to enter injured tissues from the vasculature (Liew et al, 2019). In the lungs, it was

observed using intravital microscopy (IVM), that neutrophils also increase their crawling distances in the pulmonary capillaries to capture bacteria adhered to the lung endothelium (Yipp et al, 2017). In addition, it has been observed that monocytes display patrolling behavior as a surveillance mechanism throughout the circulation. For example, monocytes were recorded to displace at 36 μ m/min in the endothelium of carotid arteries, and 9 μ m/min in the mesenteric venules (Buscher et al, 2017). Contrastingly, motility has not been as well elucidated in AMs. In the lungs, Westphalen *et al.* observed that AMs remained stationary at fixed alveolar locations for up to 4 hours, suggesting that AMs were sessile (Westphalen et al, 2014). However, this idea contradicted with a finding in 1993 where Peao *et al.* used calcium tungstate to label AMs and observed that some AMs were located at the Pores of Kohn, suggesting that AMs migrated through the Pores of Kohn (Peao et al, 1993). Further, the practicality of sessile AMs has also been challenged. Due to the higher number of alveoli in comparison to AMs, not all alveoli contain AMs at any given time, raising the question of how each alveolus can be equally protected from pathogens. Recently, our lab utilized IVM to observe the AMs in their natural environment at homeostasis in a living mouse. It was observed that AMs migrated up to 90 μ m within 2 hours (Neupane et al, 2020). This behavior was suggested to be an important mechanistic approach for AMs to perform their homeostatic functions of patrolling the alveolar spaces (**Figure 1.1**). In addition, this behavior was also important for chemotaxis toward inhaled bacteria as AMs were observed to clear basal levels of bacteria from the lung very rapidly without inducing neutrophil recruitment.

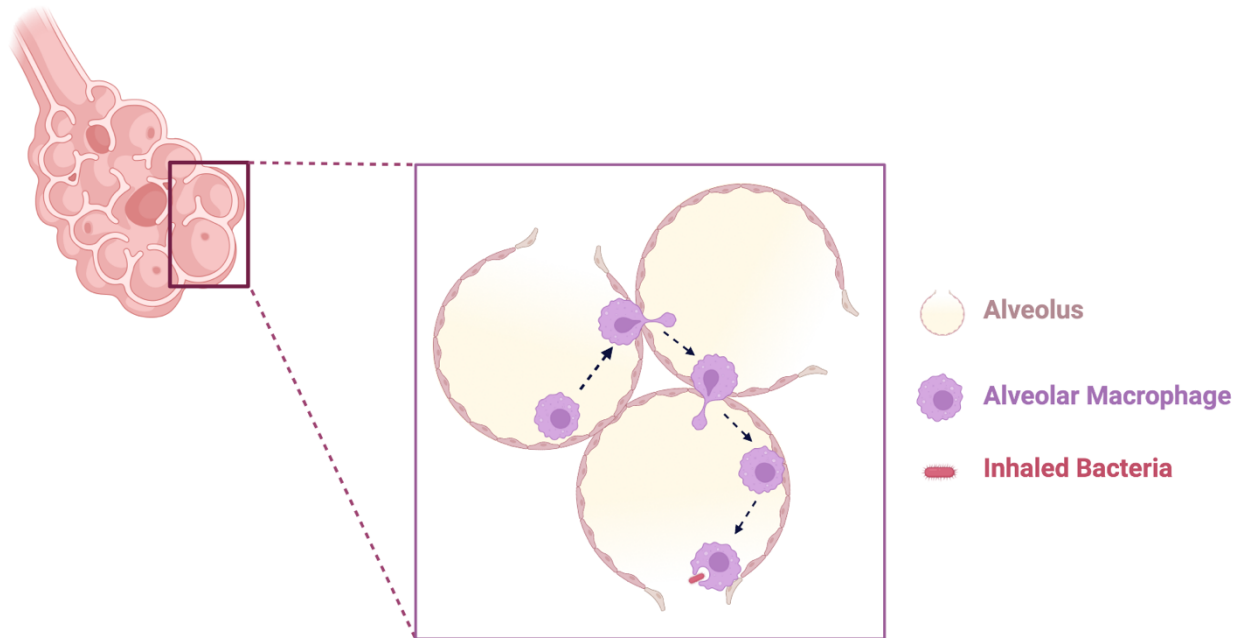


Figure 1.1. AM migrate across alveoli and engulf foreign particles and clean the alveolar space.

AMs migrate from alveolus to alveolus during homeostasis through the Pores of Kohn. This movement is critical for AMs to perform their role of cleaning the alveolar space of cellular debris, foreign particles, and apoptotic cells.

1.2.3 Immune surveillance: Keeping the alveoli in check

During physiological conditions, AMs maintain pulmonary homeostasis by clearing surfactant, debris, and unwanted particles in the alveolar space. To perform these roles, AMs possess a high phagocytic capacity and actively limit the secretion of pro-inflammatory cytokines to prevent activating the adaptive immune system. Thus, this enables the AMs to patrol and clean alveolar spaces in a silent manner that minimizes lung inflammation. The homeostatic functions of AMs to clear surfactant, limit lung inflammation, and respond to respiratory

pathogens will be highlighted in the sections below.

1.2.3.1 Catabolizing and clearing surfactant from the alveolar space

Surfactant is produced by the AEC2s and reduces the surface tension in the alveolar lumen to maintain alveolar compartment stability and prevent alveolar collapse (Knudsen et al, 2018). It lines the alveolar epithelium as an active thin and continuous film, and its homeostasis is crucial for lung function (Goss et al, 2013; Veldhuizen et al, 2000; Schürch et al, 1982). However, excessive accumulation of surfactant could decrease the integrity of the alveolar space and lead to pulmonary alveolar proteinosis (PAP) and respiratory failure (Carey et al, 2010). AMs play a crucial role of regulating the level of surfactant in the alveolar lumen and are responsible for up to 40% of surfactant catabolism (Miles et al. 1985; Guilliams et al, 2013). To fulfill this function, AMs utilize the GM-CSFR-PPAR- γ axis. Engagement of the GM-CSFR on the surface of AMs leads to the expression of the nuclear receptor PPAR- γ , which in turn regulates the expression of genes involved in lipid intake and catabolism (Baker et al, 2010; Gautier et al, 2012).

1.2.3.2 Dampening the immune response in the alveolar space

At steady state, AMs maintain an immunosuppressed form and induce negative regulatory signals to minimize AM activation against manageable inhaled material. Some of the well-known inhibitory surface receptors expressed by AMs include the TGF- β R, IL-10R, and signal regulatory protein alpha (SIRP α), which will be individually discussed below.

TGF- β R is expressed on AMs and responds to TGF- β , a cytokine produced by a variety of lung cells including AMs thereby suggesting both paracrine and autocrine activity. It has been suggested that TGF- β is critical to preventing lung emphysema and widespread lung inflammation (Morris et al, 2003). The secretion of TGF- β by AMs also induces forkhead box P3 (FOXP3) expression in naïve and activated CD4⁺ T-cells that then suppresses T-cell activity (Hussell and Bell, 2014). IL-10 is an anti-inflammatory cytokine that is involved in immunosuppression and homeostasis (Bonfield et al, 1995; Fernandez et al, 2004). This cytokine is constitutively expressed by pulmonary epithelial cells. AMs express IL-10R and its activity with IL-10 is primarily associated with the STAT3-induced expression of SOCS3 which prevents expression of pro-inflammatory genes (Takeda et al, 1999; Yoshimura et al, 2007). SIRP α is expressed on the AMs and activated by ligands including CD47, surfactant proteins pulmonary surfactant-associated protein A (SPA) and surfactant-associated protein D (SPD). The SIRP α -CD47 axis creates an inhibitory signal for phagocytosis, acting as a “do-not-eat-me” signal to block phagocytosis of healthy cells (Barclay et al, 2014). As well, surfactant protein A (SPA) and surfactant protein D (SPD) are also ligands for SIRP α which as an example inhibits LPS-induced production of pro-inflammatory cytokines (Haczku et al, 2008; Gardai et al, 2003).

1.2.3.3 AM response against *Staphylococcus aureus*

Staphylococcus aureus (*S. aureus*) is gram-positive commensal bacteria and *S. aureus* infection accounts for approximately 20,000 deaths in the U.S each year (Wertheim et al, 2005; Kourtis et al, 2019). Although *S. aureus* colonize the skin and mucosa, the anterior nares are the most frequent site for *S. aureus* invasion. Through airborne transmission, *S. aureus* commonly disperse into the nose and spreads to the lower respiratory tract. To ensure the sterility of the

lower airways, the innate immune cells in the alveoli immediately respond to eliminate the bacteria and prevent its entrance into the bloodstream.

Neutrophils and AMs have been suggested to be crucial for *S. aureus* clearance. In the case of neutrophils, it has been shown that these cells clear *S. aureus* bacteria through a NADH-oxidase-dependent manner, and via neutrophil extracellular traps (Ellson et al, 2006; Brinkmann et al, 2004). It has been suggested previously that innate clearance of the bacteria only requires neutrophils, but not macrophages. However, others have challenged this notion showing that although neutrophils are important for bacterial clearance, the absence or depletion of AMs resulted in reduced killing of the bacteria and enhanced bacteria-induced mortality (Sun and Metzger, 2008; Yajjala et al, 2016; Martin et al, 2011; Kitur et al, 2016). Moreover, neutrophils are not readily available in the alveoli and are recruited from the vasculature into the lungs via the two CXC chemokines: MIP-2 and KC. In contrast, the AMs conveniently reside in the alveoli tissue and are readily available to respond to the bacteria. It has been shown that macrophages are in fact the first responders to clear bacteria through an NADH-oxidase-dependent and -independent manner. In our lab, we have used IVM and observed that AMs crawl toward *S. aureus* to engulf the bacteria. Interestingly, it was observed that when the bacteria dosage was under 4 million CFUs, AMs cleared the bacteria within the first 2 hours of infection without the need for neutrophils. When AMs were depleted, massive neutrophil recruitment occurred during this time frame and induced unnecessary lung inflammation. This result demonstrates the importance of AMs to clear basal levels of pathogen while mitigating tissue damage (Neupane et al, 2020).

AMs have key molecules to deal with *S. aureus*. One mechanism of *S. aureus* clearance by AMs is the interaction between the macrophage and surfactant protein A (SPA). As a member of the C-type lectin family, SPA acts like an opsonin and binds to *S. aureus* and CD11b of AMs to facilitate *S. aureus* phagocytosis (Kurannuma et al, 2004; Sever-Chroneos et al, 2011). Macrophage receptor with collagenous structure (MARCO) is another component of AM-mediated phagocytosis of *S. aureus* (Arredouani et al, 2005). It has been shown that SPA or MARCO-deficient mice exhibited reduced clearance and phagocytosis of *S. aureus* (Palecanda et al, 1999; Zhou et al, 2008).

1.2.3.4 Influenza A Virus (IAV) pathogenesis and AM response

Influenza A virus (IAV) is a single-stranded negative-sense RNA and is one of the leading causes of mortality worldwide (WHO, 2012). Different from bacterial infection, IAV infects by inserting its genome into host cells, leading to replication of the viral genome and dissemination inside the host cell. As the virus travels down the respiratory tract, it primarily targets the epithelial cells lining the bronchi. This is because the hemagglutinin (HA) protein expressed on the IAV targets sialic acid receptors which are predominantly expressed on the surface of epithelial cells. Once the virus replicates inside the epithelial cells, virions are released back into the airspaces to travel further down the respiratory tract. In the alveoli, IAV targets the alveolar epithelial cells and can induce direct destruction of the epithelium lining. This process determines the lethality of IAV infection as epithelium damage impairs gas exchange and increases secondary pathogen infection (Cardani et al, 2017). *In vivo* studies using murine models have associated the severity of IAV infection with the degree of alveolar epithelial cell destruction (Sanders et al, 2013; Brandes et al, 2013).

In response to IAV, AMs are essential for protection against lethal infection. It has been shown on multiple occasions that AMs play a key role in modulating IAV infection. The absence of AMs significantly increase morbidity and IAV-induced respiratory failure (Schneider et al, 2014; Kim et al, 2008; Purnama et al, 2014). Interestingly, the level of adaptive immune response is independent of AM presence as observed by an intact IAV-induced T and B cell response after AM ablation (Schneider et al, 2014; Purnama et al, 2014). Therefore, how AMs affect the severity of IAV infection remains to be elucidated. In 2017, Cardani *et al.* observed that AMs inhibit infection of alveolar epithelial type I cells (AEC1), preventing lethal influenza pneumonia (Cardani et al, 2017). However, how this occurs mechanistically also remains to be explored.

Despite viral dissemination inside the respiratory tract, >95% of deaths in the 1918 influenza pandemic were caused by post-influenza bacterial infections (Russell et al, 2008). During the 1957 and 2008 pandemics, it has been recorded that half of the patients admitted to the hospital had evidence of bacterial coinfection, specifically with *S. aureus* or *Streptococcus pneumoniae* (*S. pneumoniae*) (Louria et al, 1959; Gill et al, 2009). These records suggest that IAV can indirectly induce immunosuppression in the host which increases host susceptibility to secondary bacterial infections. It is also possible that viral replication in the alveolar epithelial cells lead to airway epithelium damage which increases attachment sites for bacteria (MacCallum et al, 1921; Opie et al, 1921). Additionally, AMs play a critical role in bacterial clearance, and the increase in bacterial susceptibility post-IAV infection also has been suggested to be due to 1) decreased AM phagocytic ability, 2) loss of AMs (only in the BALB/C mice

strain), or 3) AM paralysis, inhibiting the chemotaxis towards bacteria (Sun and Metzger, 2008; Califano et al, 2018; Ghnoeim et al, 2013; Neupane et al, 2020).

1.3 Self-replenishment of tissue-resident macrophages

1.3.1 Self-replenishment of TR-AMs through local proliferation

Tissue-resident macrophages possess a high proliferative capacity and are known to self-renew with minimal contribution from circulating monocytes. Microglial cells are an excellent example of an independent self-renewing population, as are Langerhans cells and Kupffer cells (Palucka et al, 2006). Interestingly, it has been shown that Langerhans cells and microglia can locally repopulate even after tissue injury (Ajami et al, 2007; Merad et al, 2002). However, this self-renewal ability does not apply to all tissue-resident macrophages. For example, it has been shown that gut macrophages and dermal macrophages are constantly replaced by circulating monocytes (Liu et al, 2019). The reason behind why some tissue-resident macrophages can locally repopulate despite ablation, whilst some are replaced by monocyte-derived macrophages remains an area to be explored.

AMs have been shown to have high self-renewing ability. This proliferating ability is dependent on macrophage colony-stimulating factor (M-CSF) and IL-1 α (Davies et al, 2013; Francois et al, 2015). Early studies demonstrated using *in vivo* and *in vitro* models, the replicative capacity of AMs that fill an empty niche in murine models (Tarling et al, 1987; Nakata et al, 1999; Lehnert et al, 1992), as well as in humans (Nakata et al, 1999). Using depletion models such as diphtheria toxin and clodronate liposomes to eliminate TR-AMs, Hashimoto *et al.* demonstrated that TR-AMs fully repopulate the alveoli independently of

monocytes (Hashimoto et al, 2013). Further, it was shown recently that following an adenovirus infection, TR-AM numbers were reduced but returned to basal levels a month after infection (Yao et al, 2018).

Although TR-AMs are capable of self-renewal, it has been recently suggested that TR-AMs are replaced by MO-AMs over time. However, the lack of tools limits our ability to distinguish tissue-resident and monocyte-derived macrophages in the lung. Further, although it has been shown that circulating monocytes are able to differentiate and adopt an identical function and characteristic as AMs, the amount of time that MO-AMs require to adopt the niche of TR-AMs is not delineated. Moreover, a systematic comparison of TR-AMs and MO-AMs is unavailable, limiting our understanding of why TR-AMs self-renew versus turnover.

1.4 Monocyte-derived Alveolar Macrophages (MO-AMs)

1.4.1 Origin: Monocytes

Monocytes are a heterogenous population of cells that circulate the bloodstream and generally recruit to tissues and give rise to tissue macrophages under inflammatory conditions. Post-natal monocyte development depends entirely on M-CSF, which has a short half-life of 20 hours (Cecchini et al, 1994; Dai et al, 2004). Monocytes are generated in the bone marrow from hematopoietic stem cells (HSC). HSCs give rise to a diverse range of hematopoietic cells and in the development of monocytes, they first develop into the common myeloid progenitor (CMP) cells (Zhu et al, 2016). CMPs then differentiate into granulocyte-monocyte progenitors (GMP) and monocyte-DC progenitors (MDP) (Fogg et al, 2006; Liu et al, 2019). More recently, a novel intermediate was subsequently discovered to differentiate from MDP and give rise to classical

and non-classical monocytes but not DCs. This intermediate was termed the common monocyte progenitor (cMoP) (Hettinger et al, 2013). Therefore, the monocyte development pathway model has been suggested to be $CMP \rightarrow GMP \rightarrow MDP \rightarrow cMoP \rightarrow monocyte$ (**Figure 1.2**). However, this developmental pathway has been challenged recently by Yanez *et al.* who suggested that MDPs directly arise from CMPs independently of GMP (Yanez et al, 2017). In addition, through lineage-tracing tools, MDPs were shown not to arise from CMPs and can give rise to monocytes independently of cMoPs (Liu et al, 2019).

Two main monocytes have been reported in mice and humans (Geissmann et al, 2003; Passlick et al, 1989). In mice, the two common monocyte types can be differentiated through the variable expression of the lymphocyte antigen 6C (Ly6C). The Ly6C^{high} monocyte subtype is characterized by the high expression of C-C chemokine receptor 2 (CCR2), and low expression of the CX3C chemokine receptor 1 (CX3CR1) (Kratofil et al, 2016; Geissmann et al, 2003). The second monocyte subset is characterized by low expression of Ly6C (Ly6C^{low}), low expression of CCR2, and high expression of CX3CR1. It has been suggested the Ly6C^{high} monocytes represent the classical monocytes that recruit to sites of inflammation, while Ly6C^{low} monocytes serve as patrolling monocytes that circulate the bloodstream and survey the endothelium integrity (Auffray et al, 2007; Carlin et al, 2013).

The functions of the Ly6C^{high} and Ly6C^{low} monocytes continue to be studied. IVM suggested that Ly6C^{low} monocytes patrol the vasculature by crawling on the lumen side of the endothelium and play a role in early responses to inflammation and tissue and repair (Auffray et al, 2007; Carlin et al, 2013). Contrastingly, Ly6C^{high} monocytes demonstrate a higher phagocytic

capacity and mobilize from the bone marrow to sites of infection or injury. In contrast to the patrolling Ly6C^{low} monocytes, Ly6C^{high} monocytes possess pro-inflammatory and antimicrobial functions, and are crucial for fortifying the innate immune response against bacterial infections (Serbina et al, 2008). Numerous groups however have more recently reported that in many instances, the Ly6C^{high} monocyte becomes the Ly6C^{low} monocyte.

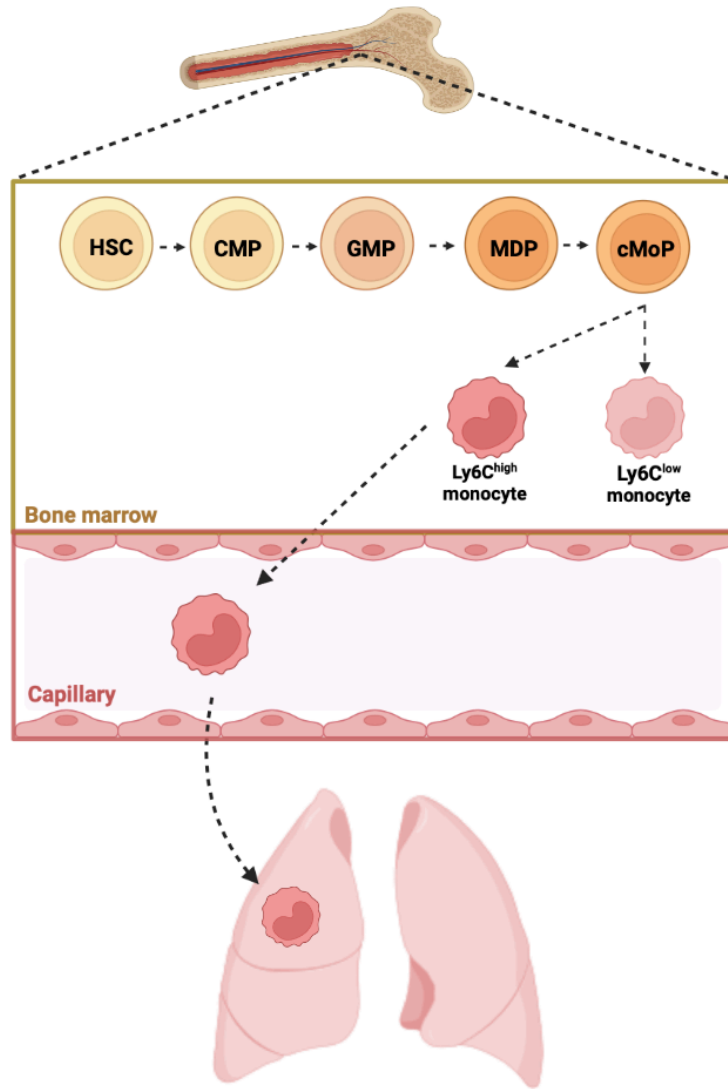


Figure 1.2. Monocyte development, recruitment, and differentiation into tissue-resident macrophages.

Monocytes arise from the bone marrow from HSCs. HSCs differentiate into CMP, followed by intermediates GMP, MDP, and cMoP, eventually giving rise to monocytes. Monocytes egress from the bone marrow and circulate the bloodstream. Ly6C^{high} monocytes infiltrate into sites of inflammation in injured or infected tissues or organs. Ly6C^{low} monocytes are patrolling monocytes in the bloodstream.

1.4.2 Recruitment of monocytes into tissues during infection

During an infection, monocytes traffic from the bloodstream to the peripheral tissues. Recruitment occurs through the CCL2-CCR2 signaling axis. During inflammation, pro-inflammatory cytokines trigger the release of chemokine CC-chemokine ligand 2 (CCL2) which attaches to receptors on monocytes (CCR2), mediating Ly6C^{high} monocyte recruitment (Tsou et al, 2007; Tsuboi et al, 2002). Interestingly, it has been demonstrated that during an infection, Ly6C^{low} monocytes can be recruited to the site of infection much earlier than Ly6C^{high} monocytes and participate in initial inflammatory response through the release of tumor necrosis factor α (TNF α) and cytokines (Auffray et al, 2007). However, in most cases, the ensuing recruitment of Ly6C^{high} monocytes provide a more prominent and robust response.

Monocyte recruitment enhances antibacterial protection in the lungs and is beneficial for the host. During *Mycobacterium tuberculosis* (*M. tuberculosis*) infection, it has been shown that although monocyte recruitment is dispensable for bacterial control at a low-inoculum, CCR2-dependent monocyte recruitment is crucial for protection at a high-inoculum (Peters et al, 2001). It was shown that the inhibition of monocyte recruitment resulted in reduced numbers of interferon gamma (IFN γ)-producing T-cells in the lungs and led to rapid death from overwhelming infection (Peters et al, 2001). This shows that although the lungs can eliminate basal levels of pathogens, monocyte recruitment is required to assist the immune response during a higher infectious dose (Scott et al, 2002; Peters et al, 2001).

In contrast to bacterial infections, monocyte recruitment during viral infections has been shown to be detrimental. For example, during IAV infection, the lack of monocyte recruitment in

CCR2-deficient mice led to a milder inflammatory response with reduced lung pathology and increased survival rates (Dawson et al, 2000; Aldridge et al, 2009). It has been shown that the absence of monocyte recruitment was associated with lower CD8⁺ T-cell recruitment to the lungs at the peak of infection. Lymphocyte recruitment into the lungs increases rapidly at day 5 post-infection and peaks at day 7. However, the excessive expansion of lymphocytes in the lungs is associated with increased lung tissue damage. This implies that unnecessary monocyte infiltration could be associated with excessive lymphocyte-induced lung tissue damage. However, as lymphocytes play a crucial role in clearing viruses, reduced lymphocyte recruitment also reduced viral clearance as the viral load was shown to be 10- to 15-folds higher in CCR2 knock-out (KO) mice than in wild-type (WT) control mice (Dawson et al, 2000). However, the reduced mortality of the WT control mice suggests that the pathological manifestation of IAV infection relies on more than just the viral load.

1.4.3 Replenishing TR-AMs with MO-AMs during inflammation

Although TR-AMs are regarded as self-renewing cells, forced ablation of these cells has led to replacement by MO-AMs. For example, the depletion of TR-AMs by IAV infection was shown to induce monocyte recruitment which led to TR-AM and MO-AM heterogeneity (Li et al, 2022; Aegerter et al, 2020). This depletion-induced MO-AM replenishment was also demonstrated following pneumococcal pneumoniae, bleomycin treatment, and murid herpesvirus 4 (MuHV-4) infection (Arafa et al, 2022; Misharin et al, 2017; Machiels et al, 2017). MO-AMs are noted to persist long-term in the lungs following recruitment. For example, MO-AM numbers progressively increased post-IAV infection, overcrowding the lung eventually occupying over 50% of the total AMs by 81 days post-IAV infection (Li et al, 2022). Similarly, following

MuHV-4 infection, the colonization of monocytes in the AM niche persisted for 28 days post-infection (Machiels et al, 2017). This AM heterogeneity was also observed after bleomycin treatment, where MO-AMs constituted 50% of the AM pool 1 year after treatment (Misharin et al, 2017).

1.4.4 Turnover of tissue-resident macrophages with age

Tissue-resident macrophages are replaced gradually by monocyte-derived macrophages with age. This process has been shown to occur rapidly in the skin and intestinal mucosa as monocyte-derived macrophages occupy up to 80% of total macrophage population by 8-weeks of age (Ginhoux et al, 2010, Liu et al, 2019). This observation was confirmed through multiple experimental approaches such as lineage tracing, parabiosis, and immunophenotyping (Bain et al, 2014). It has been postulated that a reason for this continuous turnover in the gut as well as skin compartment is due to the constant exposure to environmental pathogens and stimuli. In the case of the lungs, it is interesting that despite mirroring the situation of tissues directly exposed to the environment, local proliferation rather than monocyte replacement has been proposed for AMs. However, using lineage-tracing techniques, it has been shown that there is an increasing number of MO-AMs in the lungs with age. In 2019, Liu *et al.* demonstrated that the turnover of TR-AMs to MO-AMs gradually increased from approximately 20% to 70% by 36 weeks of age (Liu et al, 2019). Similarly, Li *et al.* used bone marrow transplant to track the origin of AMs over 47 weeks and indicated a >50% contribution of monocytes to the AM pool (Li et al, 2022). It is possible that the increase in MO-AM contribution to the AM pool could be due to the loss of proliferative capacity in TR-AMs. Using scRNA-sequencing, McQuattie-Pimentel *et al.* reported the downregulation of cell-cycle genes in AMs with advancing age (McQuattie-Pimentel, 2021).

In addition, it has been suggested that turnover of TR-AMs to MO-AMs is associated with changes in the alveolar microenvironment with age. For example, there is an age-related hypo-responsiveness of AMs to GM-CSF (McQuattie Pimentel et al, 2021). Research has also suggested that although TR-AMs are capable of self-renewal, repeated exposure to severe lung insults result in the loss of proliferative capacity and forced replenishment by monocytes. Therefore, it has been speculated that the natural turnover to MO-AMs in the lung is a result of cumulative exposure to external environmental insults. However, despite the evidence for changes in the alveoli over time, the mechanistic drive behind TR-AM to MO-AM turnover remains unclear.

1.4.5 Monocytes can perform the homeostatic roles of resident macrophages

The ability for monocytes to differentiate and perform the homeostatic roles of macrophages has been established (Yona et al, 2013; Hashimoto et al, 2013). In humans, it was shown that monocytes colonize the alveolar niche following lung transplants and adopt the functions of TR-AMs (Byrne et al, 2020). In a humanized mouse model, Evren *et al.* showed that both fetal liver and adult monocytes can develop into TR-AMs *in vivo* (Evren et al, 2021). It was also by Van de Laar *et al.* that in mice, bone marrow-derived monocytes, yolk-sac macrophages, and fetal liver monocytes were all able to colonize the empty alveolar niche and differentiate into functional TR-AMs (Van de Laar et al, 2016). In addition, Lavin *et al.* saw that monocyte precursors transplanted into the lung adopted tissue-resident-macrophage-like enhancers, indicating that the lung microenvironment dictates macrophage identity (Lavin et al, 2014). As well, the ability for monocyte-derived macrophages to adopt the roles of tissue-resident macrophages have been demonstrated in various tissue compartments. For example, monocytes

recruited during tissue injury can give rise to long-living self-renewing macrophages in the skin (Merad et al, 2002). Similarly, monocyte-derived Kupffer cells transcriptionally resembled their embryonic counterparts 1 month following diphtheria-toxin-induced Kupffer cell depletion (Scott et al, 2016). As well, monocyte-derived Kupffer cells were able to perform the homeostatic role of bacteria capture 60 days following clodronate liposome-induced Kupffer cell depletion (David et al, 2016). In the lungs, it has been shown that 1 year following bleomycin treatment, MO-AMs and TR-AMs were indistinguishable by flow cytometry with very little transcriptomic differences (Misharin et al, 2017).

1.5 TR-AMs vs. MO-AMs

1.5.1 AM markers

AMs express the macrophage-specific markers: CD64 and MerTK. They also express low levels of CD11b, but high levels of CD11c, which combines with CD18 to form an integrin important for phagocytosis of complement-opsonized particles (Hussell and Bell, 2014; Zaynagetdinov et al, 2013). These cells also express sialic acid-binding immunoglobulin-like lectin F (SiglecF). These markers together allow for the definition and tracking of AMs (Zhang et al, 2007, Mao et al, 2013).

1.5.2 The roles of TR-AMs and MO-AMs at homeostasis

At homeostasis, there has been very little difference between TR-AMs and MO-AMs. Indeed, MO-AMs can adopt an identical transcriptomic profile to TR-AMs and perform their homeostatic roles of clearing surfactant and preventing pulmonary alveolar proteinosis (PAP) (van de Laar et al, 2016). In addition, both macrophage populations were highly similar in terms

of phagocytic uptake and pro-inflammatory cytokine production in response to *Escherichia coli* (*E. coli*) (Gibbings et al, 2015). However, current techniques to distinguish TR-AMs and MO-AMs are non-specific or utilize depletion of all macrophages with clodronate liposomes and then study MO-AMs in isolation. These methods, although effective in achieving a pool of MO-AMs, are not reflective of the natural turnover of TR-AMs with age nor the rapid infiltration of monocytes following a severe infection.

1.5.3 TR-AMs and MO-AMs during respiratory infections

TR-AMs and MO-AMs have shown to differ during inflammation after monocytes are recruited following an acute inflammatory response. It was demonstrated that 3 days following LPS-induced inflammation, MO-AMs augment acute inflammation through the production of inflammatory mediators and metabolic reprogramming associated with cytotoxic and antimicrobial functions in comparison to TR-AMs (Mould et al, 2017). In contrast, TR-AMs exhibit increased expression of enzymes important in N-glycosylation pathways and the production of tricarboxylic acid cycle (TCA)-cycle intermediates, all of which are representative of anti-inflammatory and regulatory functions (Mould et al, 2017; Jenkins et al, 2011; Jha et al, 2015). Further, MO-AMs recruited during IAV infection displayed an enhanced glycolytic capacity and proliferation rate, allowing them to overcrowd the lungs and replenish the TR-AMs (Li et al, 2022). These IAV-induced MO-AMs were suggested to exacerbate IAV infection pathology as these cells expressed a high amount of pro-inflammatory factors (Li et al, 2022; Schmit et al, 2022). Interestingly, in comparison to the TR-AM-like transcriptomic profile of MO-AMs at homeostasis, the Ly6C^{high} signature was enriched in MO-AMs recruited during IAV infection, indicating that these MO-AMs retained their monocyte progenitor profile (Aegerter et

al, 2020). However, to elucidate the functionality and characteristics of already present TR-AMs and MO-AMs at homeostasis and during acute inflammation, a side-by-side comparison is required. This would simultaneously place both AMs in the same environment and test their abilities to individually respond towards inhaled particulates and pathogens. The lack of tools available prevent researchers from studying TR-AMs and MO-AMs at long-term following an inflammatory response thus, it is unknown whether these macrophages undergo permanent changes after each challenge.

1.6 Trained immunity

Trained immunity is described as memory generated by the innate immune system. For a long time, it was assumed that the innate immune system was incapable of generating memory and that each subsequent pathogen would be encountered by an identical non-specific response (Netea et al, 2016). However, it is unlikely that only advanced vertebrates that consist of an adaptive immune system are able to generate memory. In fact, it has been suggested that plants and invertebrates, harboring only the innate immune system can also exhibit the ability to provide protection against specific re-infections (Kurtz, 2005).

1.6.1 The emergence of innate immune memory

Over the past two decades, increasing evidence has documented memory in the innate immune system. In comparison to adaptive immune memory, trained immunity describes a primitive form of memory that was first evidenced in invertebrates including mosquitos, the insect *Bombus terrestris* and tapeworms that lack an adaptive immune system (Netea et al, 2020). However, many studies have also suggested innate immune memory in vertebrates. For example,

administration of the bacteria *Bacillus Calmette Guerin* (BCG) vaccine in mouse models was shown to protect against secondary bacterial infections including *Candida albicans* (*C. albicans*) or *Schistosoma mansoni* (Van't Wout et al, 1992, Tribouley et al, 1978). To explore the independence of trained immunity from the adaptive immune system, it was also demonstrated that the BCG vaccine protected against candidiasis in SCID mice (lacking B and T-cells) (Kleinnijhuis et al, 2012). Similarly, treatment with fungal ligand beta (β)-glucan has also been shown to non-specifically protect against infection with *S. aureus* (Kokoshis et al, 1978). As well, prior infection with *C. albicans* has also shown to protect against lethal candidiasis infection in RAG-1-deficient mice lacking T-cells (Quintin et al, 2012). Finally, human studies have provided supporting evidence such as using the BCG vaccine to provide protection against yellow fever (Arts et al, 2018).

1.6.2 Epigenetic modification

Trained immunity is characterized by epigenetic remodeling of innate immune cells upon encountering immune stimulating agents. Two key epigenetic marks have been identified to associate with trained immunity: 1) the acquisition of histone 3 lysine 27 acetylation (H3K27ac) at distal enhancers and the consolidation of histone 3 lysine 4 trimethylation (H3K4me3) at the promoters near the transcription start sites of stimulated genes (Netea et al, 2016). Histone acetylation removes the positive charge on the histones, decreasing the interaction between the positively charged histones with negatively charged DNA thus, uncoiling the condensed chromatin into a more relaxed structure to be more easily accessible for transcription (Gregory et al, 2001). On the other hand, histone methylation is associated with less transcription activation and more transcription silencing. In the epigenetic trademark of trained immunity, trimethylation

of histone H3 lysine 4 is associated with upregulation of transcription (Gupta et al, 2010). Upon a primary stimulation, epigenetic modifications open the chromatin, making it accessible for transcription of targeted genes. Maintenance of the increased chromatin accessibility allows for easier targeted gene expression upon re-stimulation. For example, it has been shown *in vitro* that upon removal of the primary stimulus, the latent enhancers retained their opened chromatin, enabling a faster activation of transcription and hence, gene expression (Ostuni et al, 2013).

1.6.3 β -glucan as a trained immunity tool

β -glucan is a component of the fungal cell wall and has been established as a trained immunity tool. It has been shown that β -glucan increases H3K4 trimethylation (H3K4me₃) at promoter sites of important pro-inflammatory cytokines such as TNF α , IL-6, and IL-8 by interacting with the receptor Dectin-1 on leukocytes (Noble et al, 1993; Kondo et al, 1992; Young et al, 2001). This epigenetic modulation suggests the ability of β -glucan to train innate immune cells against re-infection (Quintin et al, 2012). As briefly mentioned before, several studies have suggested the protective effects of β -glucan against subsequent infections such as *Leishmania major*, *Escherchia coli*, *Plasmodium berghei*, *Eimeria vermiformis*, *Candida albicans* and *S. aureus* (Al Tuwaijri et al, 1987, Bistoni et al, 1986, Bousquet et al, 1988, Luzio et al, 1978, Rasmussen et al, 1991, Yun et al, 1997). β -glucan interacts with receptor Dectin-1, which is expressed especially high on macrophages and dendritic cells (DC) (Brown et al, 2002, Gantner et al, 2003). Recent research has provided evidence for β -glucan as a training tool. For example, it has been shown that β -glucan results in an increase in neutrophil phagocytic capacity and reactive oxygen species (ROS) production (Rubin-Bejerano et al, 2007). As well, it has also been shown that β -glucan modulates the chromatin status of monocytes to enhance their

antibacterial activity against *M. tuberculosis* infection through IL-1 signaling (Moorlag et al, 2020). This study not only suggested β -glucan to train differentiated leukocytes, but also alter myelopoiesis and induce an expansion of the production of HSCs. Indeed, it has been speculated that although β -glucan is capable of training monocytes, the lifespan of these cells is relatively short in the circulation. Thus, attention has been directed towards the ability of β -glucan to train progenitors of the hematopoietic system. It has been shown in 2018, that β -glucan administration induces the expansion of hematopoietic stem and progenitor cells (HSPCs) (Mitroulis et al, 2018). However, since HSC's do not express Dectin-1, it has been suggested that the effects of β -glucan on the HSPCs is directed through IL-1 β and GM-CSF signaling (Yanez et al, 2017; Mitroulis et al, 2018).

1.6.4 Training alveolar macrophages

Being directly exposed to the outside world, AMs frequently encounter a variety of immunostimulants, and thus serve as excellent training candidates. Indeed, the training capacity of AMs have been well explored. For example, Yao *et al.* suggested that after an infection with adenovirus, TR-AMs attenuate the severity of *S. pneumoniae* infection by secreting CXCL1 and CXCL2 (Yao et al, 2019). This evidence was further supported in 2023, where TR-AMs infected with IAV showed higher survivability upon a lethal dose of *S. pneumoniae* infection at 30 days post-IAV infection (Wang et al, 2023). In 2020, Aegerter *et al.* suggested that MO-AMs were epigenetically remodeled following IAV infection to produce IL-6 and facilitate protection against lethal bacterial infections for up to a month post-IAV infection (Aegerter et al, 2020). In addition, MO-AMs were also shown to inhibit the development of house dust mite (HDM)-induced asthma following MuHV-4 infection and can also be remodeled to secrete CXCL9 post-

pneumonia infection (Machiels et al, 2017; Arafa et al, 2022; Guillon et al, 2020). However, the concept of AM training remains a controversial topic. In 2020, it was suggested IAV infection “trains” AMs by impairing their phagocytic ability against *E. coli* or *S. aureus* for up to 1-month post-IAV infection (Roquilly et al, 2020). As well, it has also been argued that TR-AM and MO-AM remodeling is independent of ontogeny, as TR-AMs and MO-AMs both demonstrated reduced inflammatory gene expression upon secondary bleomycin administration after IAV infection (McQuattie-Pimentel et al, 2020).

In addition to evidence demonstrating trained immunity through prior exposure to pathogenic challenges, studies have also demonstrated the ability for AMs to be trained using conventional training tools. For example, it has been shown that mice vaccinated subcutaneously with BCG induced memory in the AMs to confer protection against *M. tuberculosis* bacteria independently of CD4⁺ T-cells and monocytes (Jeynathan et al, 2022). However, this result contrasts a previous study that stated BCG vaccine effectiveness requires pulmonary administration of BCG in comparison to subcutaneous administration (Mata et al, 2021).

1.7 Rationale

AMs serve as the first immune cells that contact inhaled pathogens. Thus, they serve an important host defense that dictates the severity of respiratory infections. As distinct populations, it is important to understand the separate roles of TR-AMs and MO-AMs in modulating homeostasis in the alveoli, their responses following a respiratory pathogen threat, as well as their potential to be trained against secondary infections. However, due to the limitations of current imaging technology, TR-AMs and MO-AMs remain visually indistinguishable and the

behavior of MO-AMs to maintain homeostasis like TR-AMs remain unclear. In this thesis, a new technique will be described which allows me to separate between the two AM populations. Using IVM, in combination with the AM-selective dye, PKH26, and a new transgenic $Ms4a3^{CreTdT}$ mouse line that serves as a unique marker to label MO-AMs, visual distinction between the two AM populations was achieved. This project uses β -glucan as a training tool and is the first to simultaneously interrogate the functions of TR-AMs and MO-AMs and uncover their respective abilities to be trained against respiratory viral challenges.

1.8 Hypothesis and Specific Aims

Hypothesis:

MO-AMs are more amenable to training to generate a robust immune response against viral infections and gradually replace TR-AMs to benefit the host.

Specific Aims:

Aim 1: Study and compare the population dynamic and behavior of TR-AMs and MO-AMs under homeostatic state.

Aim 2: Study and compare the behaviors and functions of TR-AMs and MO-AMs after β -glucan treatment and IAV infection. nn

Chapter Two: Materials and Methods

2.1 Animals

Ms4a3^{Cre} mice were bred in-house under specific-pathogen free, double-barrier conditions at the University of Calgary and were a kind gift from Dr. Florent Ginhoux. These mice were kept in quarantine for 6 weeks before starting experiments for this project.

Rosa26^{TdTomato} (*Rosa26^{TdT}*) mice were bred in-house and crossed with *Ms4a3^{Cre}* to generate the *Ms4a3^{Cre}Rosa26^{TdT}* mice (Madisen et al, 2010). For controls, the WT C57BL/6 mouse strain was originally obtained from The Jackson Laboratory and bred in-house. All mice were 8-10 weeks old unless otherwise specified for all experiments used in the study and were between 18g to 28g in weight. All mice were fed autoclaved rodent feed and water *ad libitum*. Mice were age and gender matched for each experiment. All experimental animal protocols carried out in this study were approved by the University of Calgary Animal Care Committee and in accordance with the guidelines drafted by the Canadian Council on the use of Laboratory Animals.

2.2 In vivo labelling of AMs

PKH26 phagocytic dye and CellVue Claret phagocytic dye were purchased from Sigma Aldrich (Sigma Aldrich, Burlington, MA, USA) (See Table 3 for more details). Our lab previously used 0.5 μ M of the PKH26 dye for IVM experiments, and 5 μ M for flow cytometry (FACs) experiments to overcome the strong auto-fluorescence (AF) signal from AMs (Neupane et al, 2020). Similarly, 0.5 μ M and 5 μ M of CellVue Claret dye were used for IVM and FACs respectively. 100 μ M of stock PKH26 was received and diluted in Diluent B to generate a working stock. Due to the sensitivity to light, dilutions were performed in the BioSafety hood

under dark conditions. Prior to aliquoting the dye for all administrations, the dilution bottle was manually shaken for 10 seconds to disperse the dye.

2.3 Oropharyngeal administration of reagents

Mice were subjected for 2-3 minutes in a 3% isoflurane (with oxygen as carrier) enclosed space. Immediately after gasping reaches intervals of 1 gasp per 3 seconds, mice were suspended by their incisors in a 60° plane. The tongue was then extruded with the use of cotton-tip applicators and held still with a gloved finger, and the volume inserted at the back of throat. The nares were then gently closed using the tip of the cotton-tip applicator and held until the mouse took 15 long breaths. The mouse was then released and replaced into the cage until consciousness and active movement returned. This method of administration was used for all reagents listed as being given oropharyngeally.

2.4 Preparation of the lung for imaging and IVM

To visualize the behavior of AM using IVM, the Nikon multichannel spinning-disk confocal intravital microscope was used to image the lungs. The set-up was adapted from previously described work (Headley et al, 2016; Looney et al, 2011). 200mg/kg ketamine hydrochloride with 10mg/kg xylazine hydrochloride were combined and injected intraperitoneally (IP) to anesthetize the animal. The animal was then maintained on a 37°C heated pad to retain body temperature. The right jugular vein was then cannulated to administer fluorescent dyes (5 μ L) and continuous anesthetics (50 μ L every 30 minutes). The trachea was then exposed, a small incision was made and then threaded with a tube that was then attached to a mini rodent ventilator to assist with breathing throughout the imaging period. The animal was

ventilated with stroke volume of 10 μ L of compressed air (20-22%) per gram of mouse weight to maintain a respiratory rate of 130-140 breathes per minute. The positive-end expiratory pressure (PEEP) was set to 2.5-3cm H₂O. Next, the intercostal muscles between the ribs were teased apart and this created a small incision of ~1.5cm opening to expose the lungs. A small lung window was then placed between the ribs and a suction of ~20mmHg was applied to stabilize the lungs. The animal, placed on the heated pad, along with the ventilator were then placed directly under the Nikon upright microscope lens. Lung images were acquired using the 10X/0.45 NA lens. TR-AMs and MO-AMs are simultaneously visualized using two laser excitation wavelengths (561 and 635nm). Images were recorded at 1 frame per minute, over a 2-hour period time-lapse series as a z stack (20 μ m stack, 3 μ m step size). A total of two to three fields of view (FOV) were acquired for each mouse. At times when images were required to be re-focused, acquiring was stopped and continued within 1 minute. The final video parts were merged using the Nikon software. Displacement and speed of the macrophages over the 2-hour imaging period was then determined using the Imaris software.

Whilst imaging the animal, drifting was encountered where the image translated horizontally or vertically during the recording process. To accommodate for the error, the video was stopped when video drifted and re-focused on the microscope before restarting the recording session. Further, when problem persisted, optimization was conducted on the Imaris software, where points were selected at the beginning and end of the video and fixed, correcting the drift and allowing for a still video to be analyzed (see Table 4 for Imaris information).

2.5 *In vivo* depletion of AMs

Clodronate liposomes (CLL) (see Table 3) and empty liposomes was purchased as a set from Sigma Aldrich. 70 μ L CLL and empty liposomes were administered directly using the oropharyngeal method.

2.6 Collecting the bronchoalveolar lavage fluid (BALF)

Mice were euthanized in a CO₂ chamber for 1-2 minutes until heart beating ceases. Next, cutting a small incision in the trachea, a 20G catheter (Surflo) was inserted into the tracheal tube where 5mL, at increments of 0.8mL of HBSS (4°C) were used to wash, detach the cells, and collect the macrophages from the alveolar space. Total recovered volume was approximately 4.5mL, where the cells were then centrifuged at 1500rpm for 5 minutes at 4°C. The supernatant was then collected from the cell pellet and kept either for determining the BAL turbidity in a spectrophotometer or plated on blood agar plates to quantify free bacteria in the alveolar space. The remaining cell pellet was then lysed with ACK for 2 minutes, washed in 2% HBSS, spun at 1500rpm for 5 minutes at 4°C and kept on ice until staining for FACs.

For quantification of BAL fluid proteins, the BAL was spun at 1500rpm for 5 minutes and the supernatant was collected. The proteins in the BAL were then quantified using the Pierce BCA protein quantification kit (ThermoFisher) according to manufacturer's instructions.

2.7 Flow Cytometry (FACs) preparation

To prepare the animal for FACs, the mouse was euthanized in a CO₂ chamber. The BAL was extracted using the protocol explained above. Next, both lungs were collected from the animal and placed into RPMI medium to wash and remove blood and unwanted material. After

removing the RPMI fluid, the lungs were minced using scissors to increase surface area. 3mL of RPMI mixed with 0.1% Collagenase type XI (Sigma) and 0.17% of DNase I (Sigma) was then added and the mixture was incubated at 37°C for 30 minutes with rocking. The lung mixture was then poured into a 70 μ M filter and pressed using the plunger of a 3mL syringe. While doing this, the mixture was washed with 10mL of 2% BSA (in phosphate buffered saline (PBS)) and spun for 1500rpm at 4°C for 5 minutes. The supernatant was discarded, and 2mL of ACK lysis buffer (GIBCO) was used to lyse the red blood cells (RBCs) for 5 minutes, and then washed with 7mL of 2% BSA (in PBS). The solution was then spun at 1500rpm at 4°C for 5 minutes. The supernatant was removed and 2mL of HBSS is added to the lung mixture. The lung solution was then pressed through a 40 μ M filter and 100 μ L was added into 96-well plates. 100 μ L of homogenous lung solution was separately heated at 95°C for 5 minutes and vigorously vortexed to obtain a vial of dead cells as a positive control in the live-dead staining process. Ghost red viability dye is then diluted in HBSS (1/800 dilution) and used to stain all dead cells in the lung homogenous mixture and incubated at 4°C for 15 minutes. 2% BSA (in PBS) was then used to wash the cells and spun at 1500rpm at 4°C for 5 minutes. Cells were then stained with appropriate antibody cocktail at 4°C for 20 minutes (see Table 1). Fc blocking antibody (2.4G2, BioXCell) was included in antibody cocktail. FMO controls were used where appropriate. All samples were processed using the FACS Canto flow cytometer (BD) and analyzed using the FlowJo software (TreeStar).

2.8 Plaque Forming Unit (PFU) assay

PFU assay was performed to determine the viral load of the sub-lethal dose of IAV administered to mice. Madin-Darby Canine Kidney (MDCK) cells were obtained from ATCC

(ATCC, Manassas, VA, USA) (see Table 3 for more details) and stored in liquid nitrogen tank at -70°C . To thaw cells, the vial was warmed in a 37°C water bath for 2-3 minutes and immediately transferred to a BSC hood for subsequent aseptic procedures. Cells were mixed in Dulbecco's modified Eagle's medium (DMEM; Thermo Fisher Scientific, Ottawa, ON, Canada) supplemented with 10% fetal bovine serum (FBS, Thermo Fisher 395 Scientific, Grand Island, NY, USA) and 100 U/mL penicillin + 100 $\mu\text{g}/\text{mL}$ streptomycin (Pen/Strep, Wisent Bioproducts, St-Bruno, QC, Canada) – complete culture medium. Contents were grown and maintained in 75m^2 flasks at 37°C with 5% CO_2 condition. Cells were grown until 90% confluency was reached and were then detached by adding 5mL of 0.25% (w/v) Trypsin – 0.53mM EDTA solution for 5 minutes. To not agitate the cells, flasks were transported with caution and observed under a microscope to confirm detachment of cells before removing from flask. Cells were then pipetted into a 15mL canonical flask and centrifuged at 125g for 7 minutes. The supernatant was then removed, and cells were counted. A calculated $7.5\text{e}10^5$ cells/plate were gently dropped in 12-well plates and topped with 0.5mL complete culture medium. The cells were then grown overnight and checked under the microscope for 90-100% confluency before infection. The cells were then washed twice with 2mL PBS to remove all medium. IAV was then diluted in 10X serial dilutions and 100uL was gently dropped in the center of each well. 100uL PBS was used in the uninfected control well. The wells were then incubated at 37°C with 5% CO_2 for 1 hour with 15-minute shaking intervals. An overlay medium consisting of 2X MEM (Sigma Aldrich) and colloidal cellulose (Sigma Aldrich) at 1:1 ratio and 0.1uL TPCK-trypsin per mL was used. 1.5mL of overlay medium was added per well and then incubated at 37°C with 5% CO_2 for 48 hours. Lastly, cells were fixed with 10% paraformaldehyde (PFA) and incubated at room

temperature for 35 minutes. Crystal violet dye was then added and incubated for 15 minutes and dried to visualize plaques.

2.9 IAV infection

Mouse-adapted IAV (strain A/Puerto Rico/8/1934 H1N1; PR8) (ATCC) (see Table 2) was amplified in 10-day embryonated hen's egg and titrated on MDCK cells. The virus was purchased from Cedarlane Labs (Burlington, ON, CA). After quantifying the viral titer of the virus using PFU assay, 50PFU was used to infect mice. This concentration was used previously in our lab to induce a sub-lethal infection with a maximum weight loss of 20% at the peak of infection followed by steady weight recovery (Neupane et al, 2020). The stock IAV was diluted in sterile PBS to obtain desired concentration. Mice were infected with 50PFU/50 μ L in the infected group or 50 μ L of 1X PBS in the control group oropharyngeally. Weight tracking was performed at approximately 24-hour intervals to maintain consistency and remove confounding factors caused by the circadian rhythm of the animal. Mice that lost more than 20% of initial weight were euthanized. Mice were also assessed daily for visual signs of clinical disease including ruffled fur, inactivity, hunching, and huddling behavior.

2.10 *S. aureus* growth and infection in mice

Green fluorescent protein (GFP) expressing *S. aureus* (strain MW2) was grown overnight on blood agar plates at 37°C (see Table 2). Multiple single colonies were collected from the plates on the next day and washed 2 times in 1mL sterile 1XPBS. The optical density (OD)₆₀₀ was determined and subsequently used to calculate volume of dilution for desired concentration of bacteria. For FACs (no IVM was performed with *S. aureus* infections) experiments, 4 \times 10⁶

CFU or 4×10^7 CFU of *S. aureus* was directly administered to mice at staggered 10-minute intervals using the oropharyngeal method described above. Mice were euthanized at 2-hours post-infection. The BAL and lungs were either collected for FACs analysis or used for CFU assay performance. For bacterial CFU assays, the BAL was spun down at 1500rpm for 5 minutes, and the supernatant was collected. Serial dilutions of BAL supernatant were plated on blood agar plates and incubated overnight at 37°C in 5% CO₂. Colonies were counted and calculated as CFU per organ.

2.11 β-glucan administration

β-glucan (β-1,3-(D)-glucan) was purchased from Sigma Aldrich (Sigma Aldrich, Burlington, MA, USA). 1mg of β-glucan dissolved in 200μL 1X PBS or PBS alone were injected IP to mice and FACs was used to quantify TR-AMs and MO-AMs at 5 and 14 days after injection.

2.12 Experimental protocol for comparing TR-AMs and MO-AMs at homeostasis

For all IVM experiments to compare TR-AMs and MO-AMs at homeostasis, 75μL of CellVue Claret dye was administered oropharyngeally to mice at least 5 days prior to imaging. This is to confirm that any inflammation induced by the dye resolves before subsequent treatment of the lungs. 5 days after CellVue Claret dye administration, the behavior of the blue (TR-AM) and purple (MO-AM) macrophages was determined using IVM.

For all FACs experiments, the BAL and lungs were collected using the protocol described above and stained using the appropriate antibodies. The markers used to identify

general AMs were (CD45⁺, CD11b⁻, CD11c⁺, MerTK⁺, CD64⁺, SiglecF⁺, Ly6G⁻, Ly6C⁻) (see Table 1 for more details). TdTomato (TdT) fluorescence was used to distinguish between TR-AMs and MO-AMs as TR-AMs were TdT⁻ and MO-AMs were TdT⁺.

2.13 Statistical analysis

Statistical analysis was performed using the GraphPad-Prism software (Table 4). Data are expressed as the arithmetic mean \pm SEM. A student's t-test was used to determine the significance between two means. For multiple comparisons, assessing means among multiple groups, one-way ANOVA with Bonferroni correction was performed. For group comparisons, two-way ANOVA with Tukey's multiple comparison test was performed. A p-value ≤ 0.05 was considered statistically significant.

Chapter 3. The Turnover and Behavior of TR-AMs and MO-AMs at homeostasis

3.1 Results

3.1.1 Turnover of TR-AMs to MO-AMs increase with age

In comparison to the gut and dermis, the lung tissue was thought to be a closed system, where macrophages self-maintain locally throughout lifetime with minimum contribution from monocytes (Hashimoto et al, 2013, Hussell et al, 2014, Liu et al, 2019). However, recent fate-mapping techniques have suggested that TR-AM turnover occurs steadily with age, but their behavior and functionality remain poorly understood. To compare the functional and behavioral differences of TR-AMs and MO-AMs, we first determined a time-point where both macrophage populations were present in the alveoli. For this purpose, FACs was used to quantify the numbers of TR-AMs and MO-AMs in mice of ages 4-weeks, 8-weeks, 16-weeks, and 40-weeks. To selectively label the MO-AMs from the AM population, *Ms4a3^{Cre}Rosa26^{TdT}* mice were used. Using the TdT expression that permanently labels *Ms4a3* expressed in monocyte progenitors, the *Ms4a3^{Cre}Rosa26^{TdT}* mice were used as a fate-mapping approach that faithfully labels MO-AMs. To label AMs, CD11c⁺CD11b⁻MerTK⁺SiglecF⁺ cells were gated and TdT expression was used in the last panel to differentiate TR-AMs and MO-AMs (**Figure 3.1A**). At 4-weeks, 0% TdT⁺ was observed in the AM population (**Figure 3.1B**). At 8-weeks, approximately 16% of the total AM population were monocyte derived. At 16-weeks, a slight increase in MO-AMs was observed. Finally, at 40-weeks, 70% of the total AM population was TdT⁺, indicating that TR-AM turnover increases with age and MO-AMs became the predominant population.

In addition to FACs, IVM was used to visualize TR-AMs and MO-AMs *in vivo*. Previously, our lab successfully used the PKH26 dye which utilizes the phagocytic ability of AMs to fluorescently label the cells with high efficiency (Neupane et al, 2020). However, since PKH26 is a red fluorescent dye, TR-AMs and MO-AMs will not be distinguished as MO-AMs are pre-labeled with red TdT. Thus, a nearly identical dye to PKH, the blue fluorescent CellVue Claret dye was used. Using the combination of CellVue Claret dye (70 μ L, 0.5 μ M) and TdT fluorescence, an increase of MO-AMs (purple) from 8-weeks (17%) to 40-weeks (81%) of age was visually observed (**Figure 3.2**).

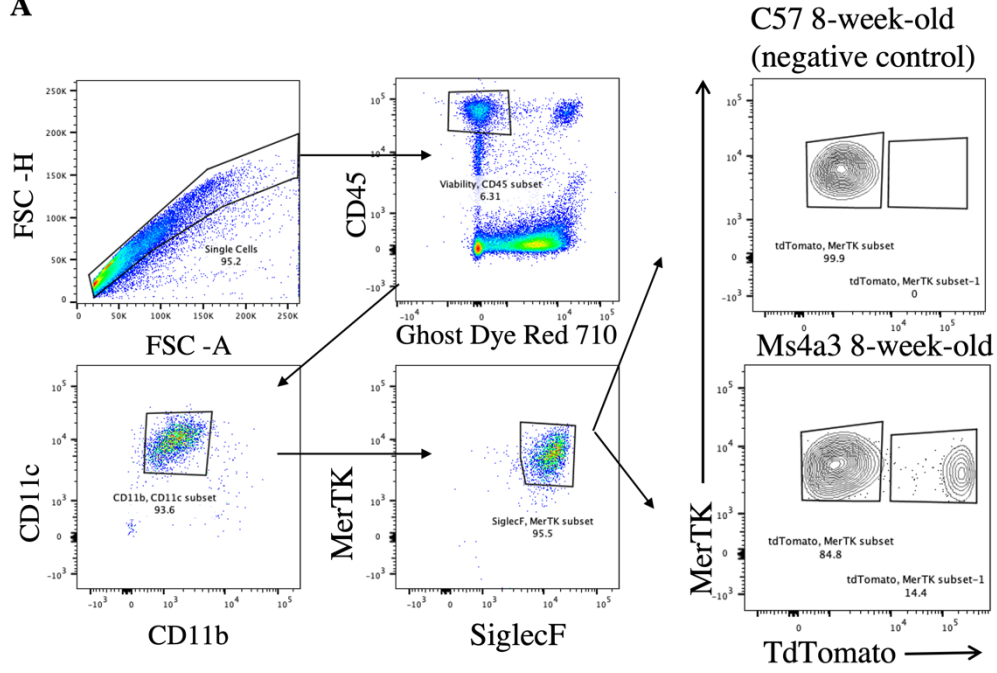
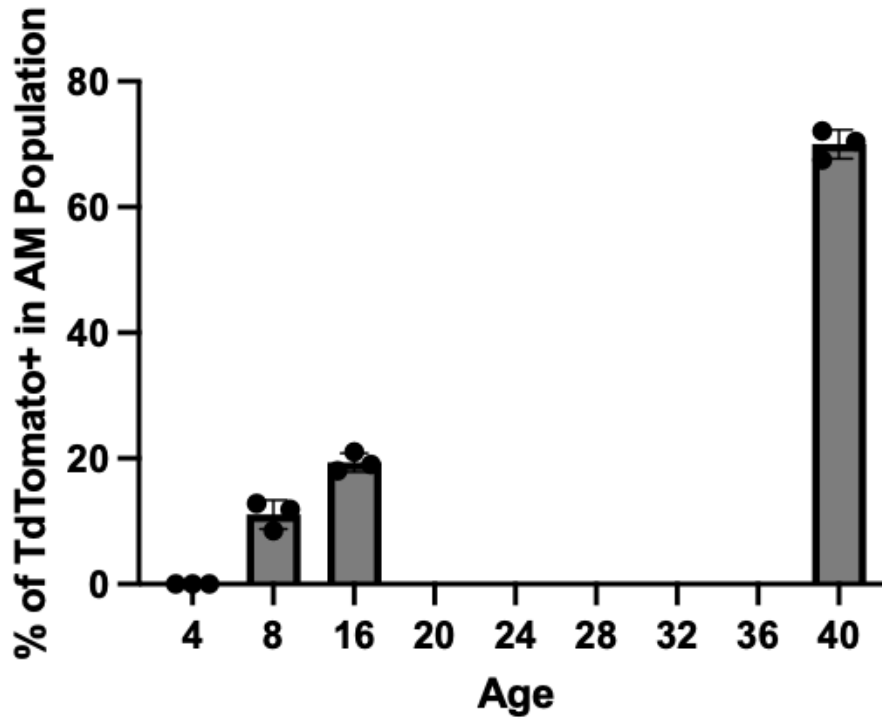
A**B**

Figure 3. 1. Percentage of MO-AMs increase in the AM population increase with advancing age.

The percentage (%) of TdT⁺ MO-AMs in the AM population. *Ms4a3^{Cre}Rosa26^{TdT}* mice at 4-, 8-, 16-, and 40-weeks of age. BALF was collected, and cells were quantified using FACs. Flow gating strategy (A) and data (B) are expressed as each data point for 3 mice per group \pm SEM.

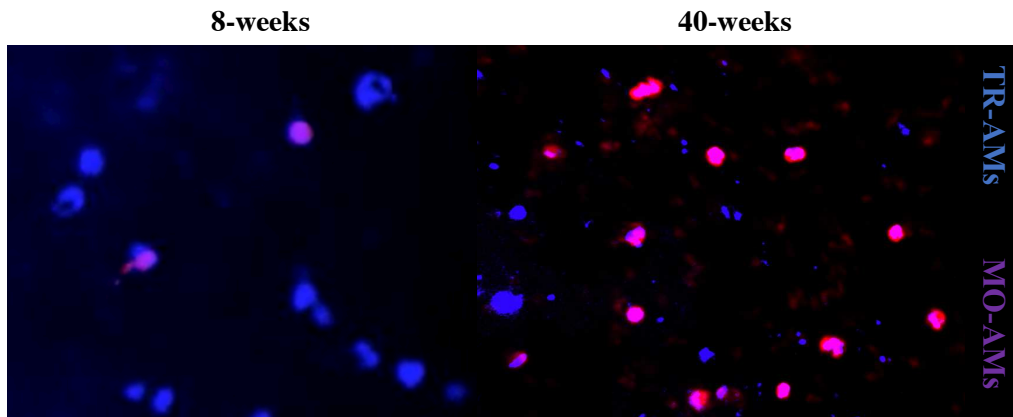


Figure 3. 2. TR-AM to MO-AM turnover cumulatively increases from 8- to 40- weeks.

IVM was used to visualize TR-AMs and MO-AMs in *Ms4a3^{Cre}Rosa26^{TdT}* mice. Results show the successful labelling of TR-AMs (blue CellVue⁺) and MO-AMs (purple TdT⁺CellVue⁺) at 8-weeks (left) and 40-weeks (right).

3.1.2 Similar net displacement of TR-AMs and MO-AMs at homeostasis at 8-weeks

To determine the behavior of TR-AMs and MO-AMs, net displacement of the macrophages were tracked over 2 hours. Unlike neutrophils that can displace $20\mu\text{m}$ in a matter of 10 minutes (Yipp, 2017), macrophages move slowly to patrol the alveolar space (Neupane et al, 2020). Therefore, 2 hours were selected as an appropriate time window to track and compare the displacements of TR-AMs and MO-AMs using IVM (**Figure 3.2**). For each mouse, 3 FOVs were randomly selected, and using the Imaris software, 20 macrophages were selected per FOV, and displacement was analyzed and recorded. This means that approximately 60 AMs were selected per mouse. Manual tracking of AMs revealed long crawling tracks, with a maximum of $88\mu\text{m}$ over the span of 2 hours. At 8-weeks, the net displacement between TR-AMs and MO-AMs are statistically similar (**Figure 3.3A**). However, at 40-weeks, MO-AMs were recorded to displace at a farther distance than TR-AMs (**Figure 3.3B**). The percentage of 8-week-old TR-AMs (**Figure 3.3C**) and MO-AMs (**Figure 3.3D**) over distributed displacements was also analyzed. At 8-weeks, TR-AMs and MO-AMs were both mostly displacing $10\text{-}20\mu\text{m}$. However, at 40-weeks, displacements were more distributed at $30\text{-}40\mu\text{m}$ in both TR-AMs (**Figure 3.3E**) and MO-AMs (**Figure 3.3F**). When comparing between TR-AMs and MO-AMs at 40-weeks, there is a larger proportion of MO-AMs displacing further ($40\text{-}50\mu\text{m}$) with a small percentage peaking at $90\mu\text{m}$.

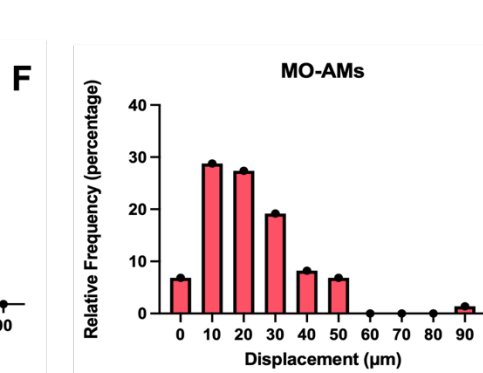
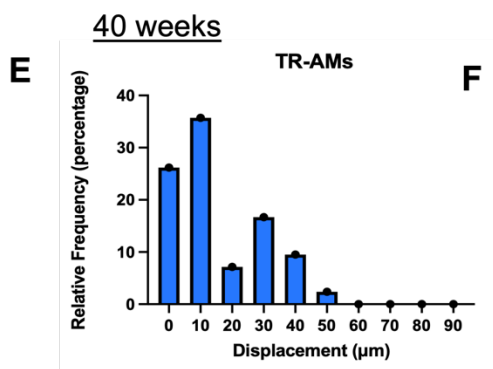
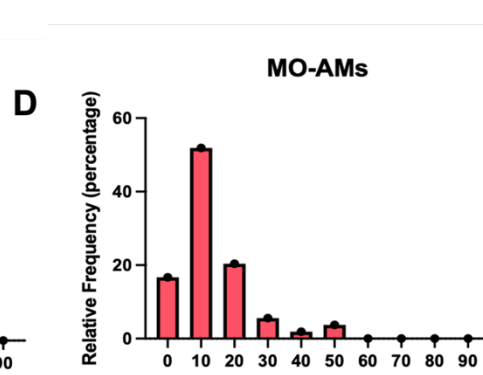
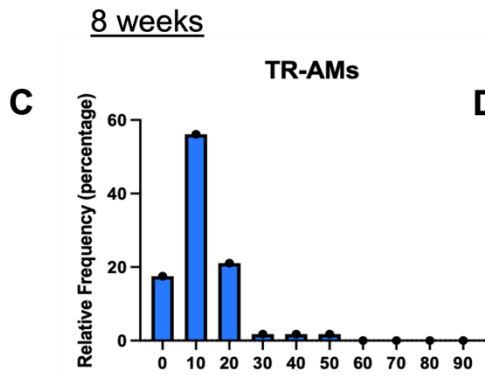
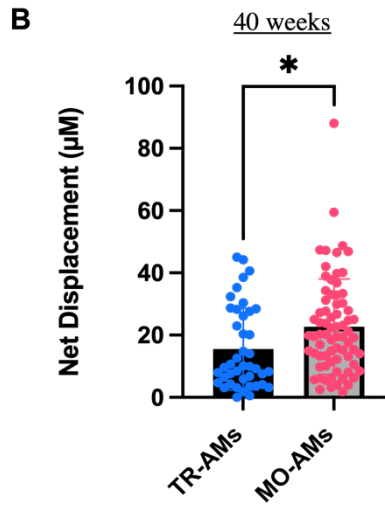
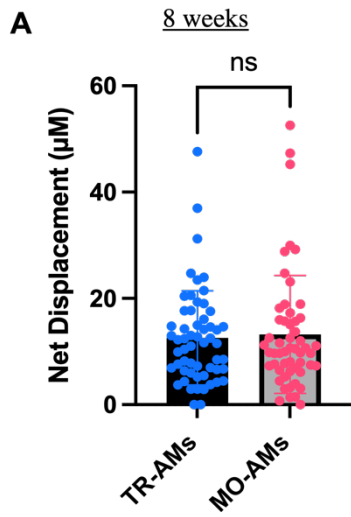


Figure 3. 3. Net displacement of TR-AMs and MO-AMs is similar in 8-week mice but different in 40-week mice.

IVM was used to visualize TR-AMs and MO-AMs in *Ms4a3^{Cre}Rosa26^{TdT}* mice and displacement of AMs were determined over a 2-hour period. At this time, 3 mice per group were used. 3 FOV were randomly selected per mouse and a maximum of 20 macrophages were selected per FOV. Results show net displacement of TR-AMs (blue) and MO-AMs (red) at 8-weeks (A), 40-weeks (B), distribution of 8-week TR-AMs (C), MO-AMs (D), and 40-week TR-AM (E), and MO-AM (F). ns = not significant and * indicates $p < 0.05$.

3.1.3 Phagocytic ability of TR-AMs and MO-AMs are similar at homeostasis

One primary function of AMs is to remove basal levels of pathogens from the alveolar space in a silent manner that avoids inducing an inflammatory response in the lung. Our lab previously showed that AM movement is crucial for patrolling the alveoli and clearing bacteria such as *Pseudomonas aeruginosa* (*P. aeruginosa*) and *S. aureus* without inducing neutrophil recruitment (Neupane et al, 2020). To determine the maximum dose of bacteria to administer without inducing neutrophil infiltration, a bacteria-dose experiment was conducted. 4×10^6 CFU or 4×10^7 CFU of *S. aureus*-GFP was administered to C57BL/6 mice. After 2 hours, neutrophil number in the lungs was determined. In comparison to 4×10^6 CFU, a significant increase of neutrophils and *S. aureus*⁺ neutrophils were observed in the lungs after 4×10^7 CFU was administered (**Figure 3.4A and 3.4B**). This indicated that while 4×10^6 CFU is not enough to recruit neutrophils to the lungs, increasing this dosage by 10-fold does signal neutrophil infiltration. Interestingly, the percentage of *S. aureus*⁺ AMs remained at ~35% and was not significantly different between the doses of 4×10^6 CFU and 4×10^7 CFU (**Figure 3.4C**). This indicated that although AMs are functional, only 30-40% of AMs were able to capture the *S. aureus*.

To compare the phagocytic abilities of TR-AMs and MO-AMs, 4×10^6 CFU *S. aureus*-GFP was administered to *Ms4a3^{Cre}Rosa26^{TdT}* mice. Animals of ages 8-weeks (**Figure 3.5A**) and 16-weeks (**Figure 3.5B**) were infected and FACs was used to determine the percentage of *S. aureus*-GFP⁺ TR-AM or MO-AM. 2 hours post-infection, the BAL was collected and processed. Using the gating strategy depicted in Figure 3.1, TR-AMs and MO-AMs were separated and GFP expression was used to identify the percentage of *S. aureus*⁺ TR-AMs and *S. aureus*⁺ MO-AMs. Since the number of TR-AMs greatly outnumber the MO-AMs at 8- and 16-weeks of age

(TR-AMs occupy ~70-80% of AM population), the relative percentage of *S. aureus-GFP*⁺ TR-AMs and MO-AMs was recorded.

Results show that at 8-weeks, approximately 30% of TR-AMs and MO-AMs were bacteria positive (**Figure 3.5A**), and at 16-weeks (**Figure 3.5B**), approximately 40% of TR-AMs and MO-AMs were able to capture bacteria within the first 2 hours of infection. Although there was an approximate 10% increase of bacteria capture by both TR-AMs and MO-AMs in the 16-weeks mice compared to 8-weeks, results suggest that both macrophages possess similar phagocytic abilities, and both are capable of crawling and capturing invading bacteria equally well.

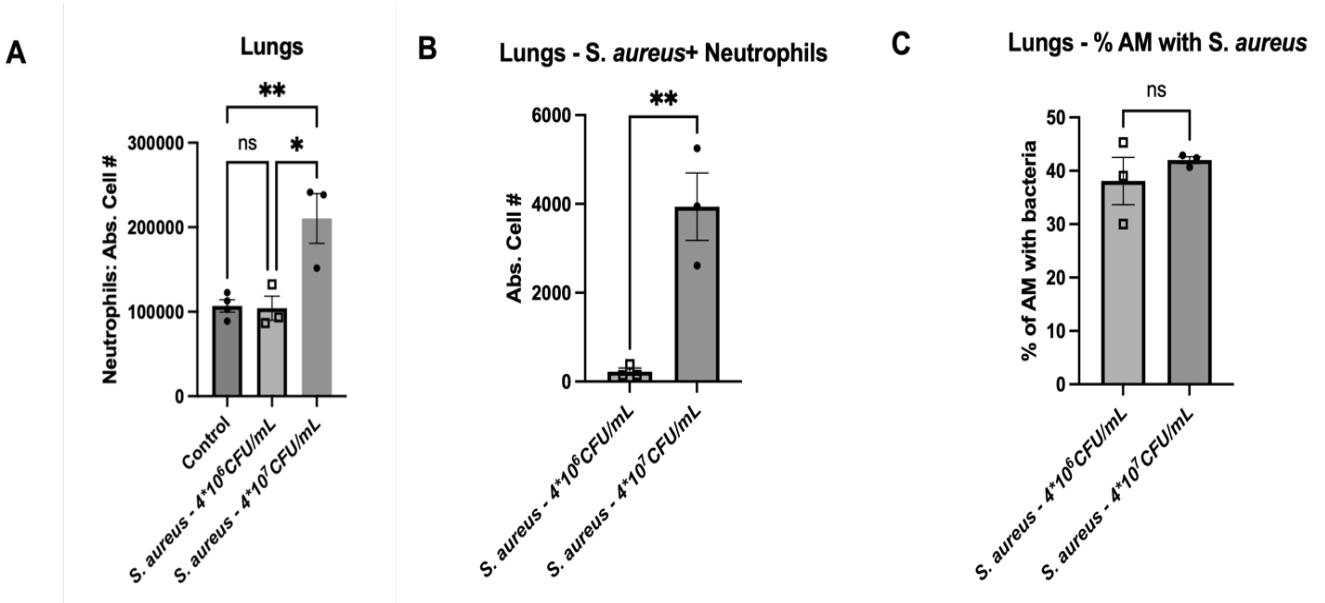


Figure 3. 4×10^6 CFU of *S. aureus* bacteria is the maximum infection dose that avoids a lung inflammatory response.

PBS (control), 4×10^6 CFU, or 4×10^7 CFU of *S. aureus* was administered through the oropharyngeal route to C57BL/6 mice. At 2 hours post-infection, lungs were collected and processed. Results show the quantification of neutrophils in the lungs (A), the number of *S. aureus*+ neutrophils (B) and the percentage of AM with bacteria (C) in control, and infections with 4×10^6 CFU, or 4×10^7 CFU of *S. aureus*. Data are expressed as one data point per animal \pm SEM for a maximum of 4 mice per group. ns = not significant and * indicates $p < 0.05$, and ** indicates $p < 0.01$.

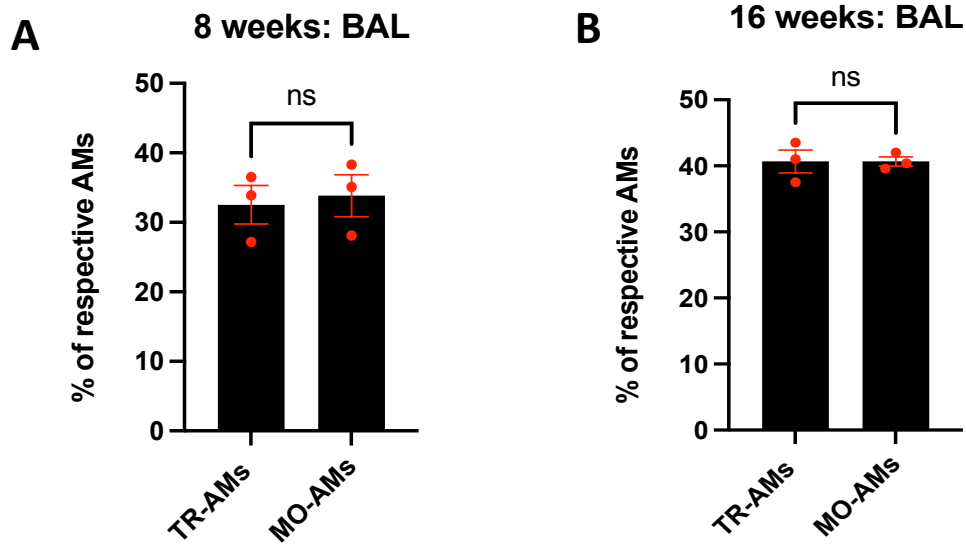


Figure 3. 5. Phagocytic ability of TR-AMs and MO-AMs is similar at 8 and 16-weeks.

8-week (A) and 16-week-old (B) *Ms4a3^{Cre}Rosa26^{TdT}* mice were infected with 4×10^6 CFU *S. aureus*-GFP⁺ bacteria via oropharyngeal administration. BALF was collected 2 hours after infection and processed. Results show the percentage of TR-AMs and MO-AMs that were GFP⁺. Data are expressed as one data point per animal \pm SEM for 3 mice per group. ns = not significant.

3.1.4 TR-AMs renew with minimal contribution from MO-AMs following clodronate-liposome-induced depletion

The previous section suggests that MO-AMs and TR-AMs behave similarly to patrol and phagocytose bacteria in the alveoli. Some researchers suggested that monocyte-derived macrophages adopt a more pro-inflammatory phenotype (Gibbins et al, 2015; Zaslona et al, 2014; Aegerter et al, 2020). To examine this, macrophage depletion was performed to induce synchronous MO-AM recruitment into an empty niche. 70 μ L of CLL was administered through the oropharyngeal route to C57BL/6 mice. At days 5 and 14 post-CLL administration, AM number was determined using FACs. At 5 days post-CLL administration, there was a 90% decrease in the AM number in comparison to the control group indicating substantial macrophage depletion. At 14 days post-CLL administration, macrophage numbers have increased to approximately 60% of the AMs in the control group (**Figure 3.6A**).

To quantify the TR-AMs and MO-AMs post-CLL administration, the same experiment was repeated in *Ms4a3^{Cre}Rosa26^{TdT}* mice. Surprisingly, at 14 days post-CLL, it was noted that the TR-AMs had not been replenished with monocytes and remained the predominant population of the total AM pool (**Figure 3.6B**). The percentage of TR-AMs in the total AM pool calculated from Figure 3.6B was 70.5% and 81.5% in the control and CLL- treated group respectively, while MO-AM percentages were calculated to be 29.5% and 18.5% respectively (**Figure 3.6C, 3.6D**).

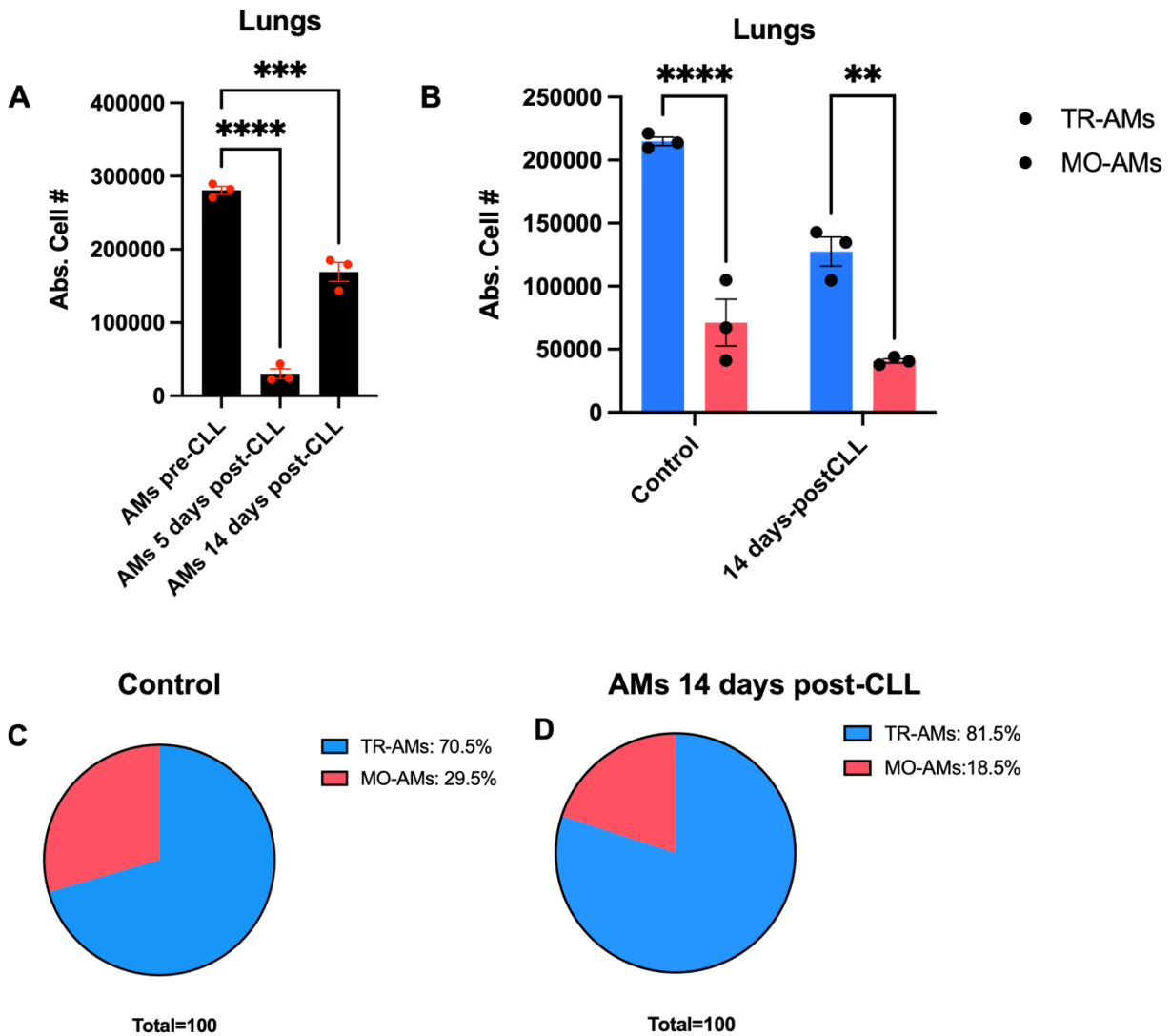


Figure 3. 6. Alveolar macrophage numbers recover 60% by 14 days post-CLL treatment and are predominantly TR-AMs.

70 μ L of CLL was administered via the oropharyngeal route to C57BL/6 and *Ms4a3^{Cre}Rosa26^{TdT}* mice. At 5 days and 14 days post-CLL treatment, the AMs were quantified. Results show total AM numbers in C57BL/6 mice at 5 and 14 days post-CLL treatment (A), and the total TR-AMs and MO-AMs number at 14 days post-CLL treatment in *Ms4a3^{Cre}Rosa26^{TdT}* mice (B). Data are expressed as one data point per animal \pm SEM for at least 3 mice per group. Results also show the

proportion of TR-AMs (blue) and MO-AMs (red) at pre-CLL (C) and 14 days post-CLL (D). ** indicates $p < 0.01$, *** indicates $p < 0.001$, and **** indicates $p < 0.0001$.

3.1.5 BAL Turbidity before and 14 days after clodronate administration is not significantly different

Following CLL administration, it was observed that the replenished AMs consist predominantly of TR-AMs. To determine if these replenished AMs can perform like mature AMs, BAL turbidity was determined. Turbidity measures the level of protein, debris, and lipid in the alveoli, thus, indicating the efficiency of AMs to “clean” the alveolar space. To determine the BAL turbidity, BAL supernatant was collected at 14 days post-CLL treatment, and the optical density 600 (OD600) was determined. Surprisingly, the OD600 in the BALF was not significantly different between control and 14 days post-CLL treatment. This indicated that under homeostatic conditions, the ability of AMs to perform at least one function was not impaired (**Figure 3.7**).

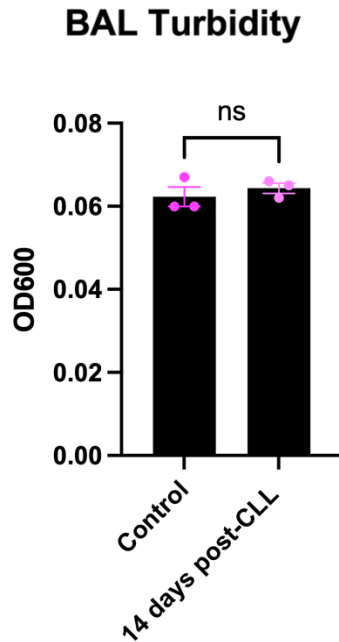


Figure 3. 7. Optical density 600 (OD600) (turbidity) of BAL supernatant remains similar at 14 days after clodronate liposome treatment.

70 μ L of CLL (CLL day 14) or saline (control) were administered via the oropharyngeal route to C57BL/6 mice. At 14 days post-treatment, BAL turbidity was identified. Results show OD600 measurement of BAL fluid turbidity of saline, control (left) and clodronate (right) treated mice.

Data are expressed as one data point per animal \pm SEM for 3 mice per group. ns = not significant.

3.1.6 Phagocytic ability of TR-AMs and MO-AMs remain the same post-CLL depletion

To further determine if replenished TR-AMs and MO-AMs can perform like mature AMs, bacteria were given to assess phagocytic ability. 14 days following CLL administration to *Ms4a3^{Cre}Rosa26^{TdT}* mice, *S. aureus* – GFP was administered. 2 hours post-infection, FACs was used to quantify the percentage of TR-AMs and MO-AMs that have captured bacteria. In the control group, approximately 25% of TR-AMs and MO-AMs captured bacteria, this percentage had not changed post-CLL (**Figure 3.8A**). However, in comparison to the control group, mice that have been treated with CLL after 14 days showed a higher bacterial burden (**Figure 3.8B**). As well, neutrophil recruitment was also higher in the BALF in mice at 14 days post-CLL treatment (**Figure 3.8C**). This result demonstrates that although the phagocytic ability of TR-AMs and MO-AMs were not inhibited, the reduction of bacterial clearance and increase in neutrophil recruitment may suggest an impairment of bacteria killing. Together, these data suggest that at 14 days post-CLL treatment, TR-AMs and MO-AMs are not yet able to perform the full functions of mature AMs.

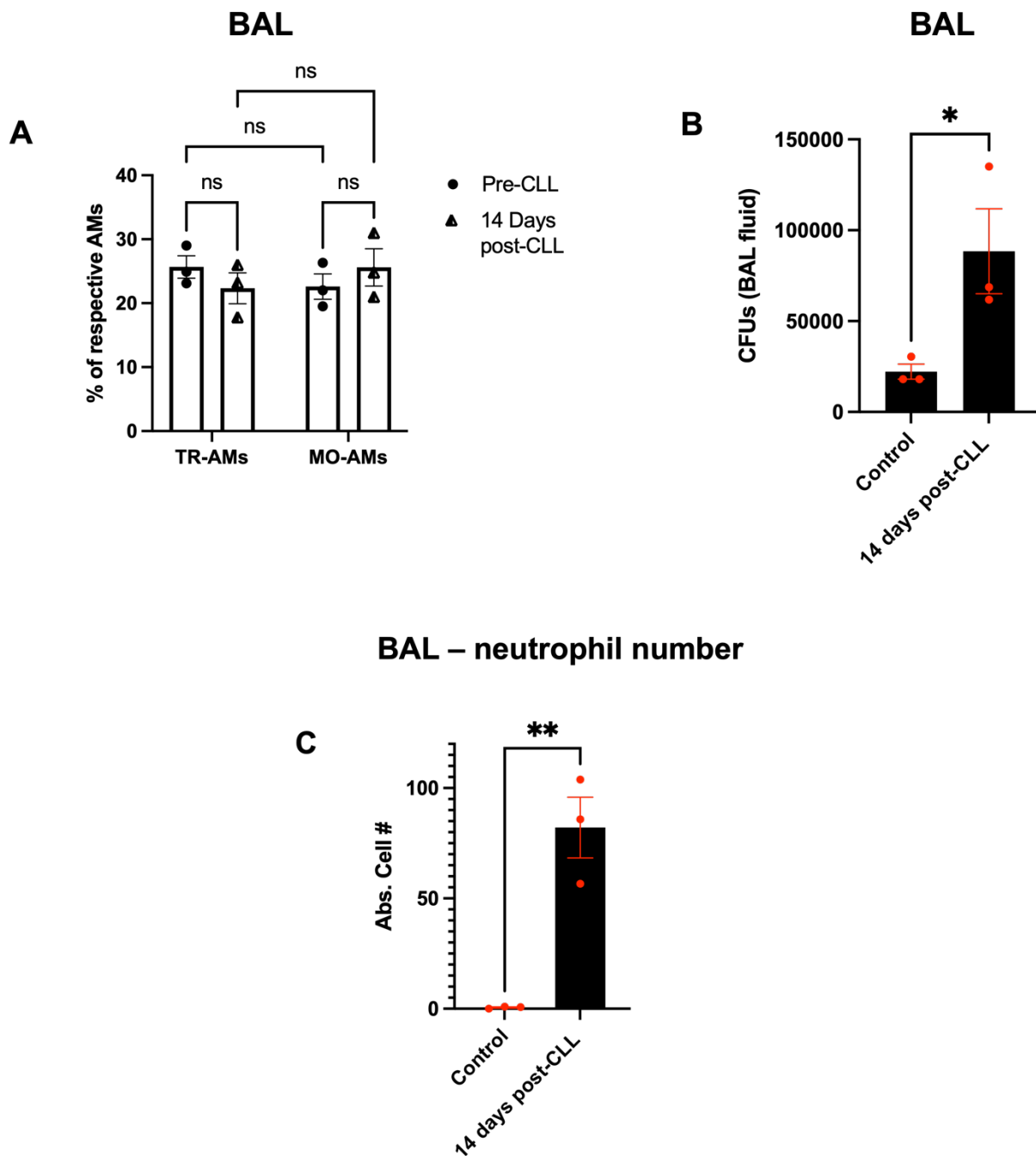


Figure 3. 8. Percentage of TR-AMs and MO-AMs with bacteria remain the same. CFU and neutrophil number in the BAL after *S. aureus* infection after clodronate liposome treatment.

70 μ L of CLL were administered via the oropharyngeal route to *Ms4a3^{Cre}Rosa26^{TdR}* and C57BL/6 mice. At 14 days post-treatment, 4×10^6 CFU of *S. aureus* was administered. At 2 hours post-

infection, BALF was collected for FACs and the BALF supernatant was plated. Results show the percentage of macrophages with bacteria (A), quantification of CFU, and neutrophil number in the BAL in control (left) and clodronate treated mice (right) (B). Data are expressed as one data point per animal \pm SEM for 3 mice per group. ns = not significant, * indicates $p < 0.05$, and ** indicates $p < 0.01$.

3.2 Discussion

In this study, we observed that although TR-AMs dominate the AM population until at least 16-weeks of age, MO-AMs steadily grow in population. By adulthood, we observed a shift of TR-AM to MO-AM ratio, with a turnover of 70% by 40-weeks of age. Although TR-AMs and MO-AMs are ontogenically distinct macrophage populations, they demonstrate similar crawling and migratory behaviors, and similar abilities to phagocytose foreign bacteria at 8- and 16-weeks of age. We also showed that TR-AMs remain the predominant AMs that replenish the empty alveolar niche thus, suggesting that TR-AMs replicate locally following massive depletion. In addition, we also showed that replenished AMs following depletion can phagocytose inhaled bacteria as well as clean the alveolar space of surfactant, debris, and lipids.

It has only been recently suggested that monocytes replenish TR-AMs at physiological state. Using the *Ms4a3^{Cre}Rosa26^{TdT}* mouse model, Liu *et al.* tracked tissue-resident macrophage turnover in multiple organs (Liu et al, 2019). For microglia, epidermal Langerhans cells and liver Kupffer cells, no turnover was observed. On the other hand, monocytes rapidly infiltrated the colon and small intestines by 8-weeks of age and differentiated into macrophages that plateaued at 80% by 36-weeks of age (Liu et al, 2019). In the lungs, Liu *et al.* showed a gradual replacement of TR-AMs by MO-AMs with age, reaching approximately 70% by 36-weeks of age. This contrasts with various lung studies that suggest TR-AM self-renewal over the lifetime. For example, using a fate-mapping technique to label monocyte progenitors, and a parabiosis model, Hashimoto *et al.* demonstrated the lack of monocyte contribution in the AM pool of adult mice (Hashimoto et al, 2014). However, these authors only used mice of 8-12 weeks of age, whereas our data and that of Liu *et al.* would indicate that most of the TR-AM turnover occurs

after 12 weeks (Liu et al, 2019). Similarly, using chimeric mice, McQuattie-Pimentel *et al.* combined radiation with thoracic shielding and monitored the AM ontogeny over the lifespan. The authors showed that a small population of MO-AMs populated the lungs but remained steadily low over the lifetime (McQuattie-Pimentel et al, 2021). However, this model of using chimeric mice uses techniques that disturb or damage the system and is vastly different from the natural turnover that our study uses. Other authors such as Yona *et al.* and Clausen *et al.* have utilized the *Cx3cr1^{CreERT2}* and *LyzM^{Cre}* models respectively to label and determine the contribution of monocytes in the lungs (Yona et al, 2013; Clausen et al, 1999). Both studies concluded that TR-AMs populate the alveoli independently of monocytes. However, each of these models suffer from a lack of specificity for MO-AMs (*Cx3cr1* also labels DCs cells, and *LyzM* also labels TR-AMs) and are thus subject to misinterpretation.

The turnover of TR-AMs and MO-AMs has been hypothesized to be due to the fact that the proliferative capacity of TR-AMs decrease with age. In 2021, McQuattie-Pimentel *et al.* observed significant differences in the transcriptomes of TR-AMs in young (4-6 month old) and old (18-24 months old) mice (McQuattie-Pimentel et al, 2021). Genes that encoded for “cell cycle” and “translation” were downregulated in the old compared to the young animals. Furthermore, the same authors also showed that aged TR-AMs confer resistance to GM-CSF. As TR-AMs lose the capacity to divide, they are inevitably replaced by MO-AMs. In addition, Wong *et al.* showed using gene expression studies that aging upregulates a suppressor of AM self-renewal, *C-Maf*, and downregulates genes involved in cell cycle regulation (Wong et al, 2017). A second reason behind TR-AM to MO-AM turnover is the disappearance of TR-AMs that must be replaced by MO-AMs following a severe lung injury. For example, IAV infection

and injury with bleomycin massively deplete TR-AMs, resulting in MO-AM recruitment and AM heterogeneity for months post-injury (Li et al, 2022; Misharin et al, 2018). This may hold true for multiple smaller injuries over the lifespan.

At homeostasis, TR-AMs and MO-AMs were observed to move equal distances at 8 weeks of age. A possible explanation is that despite being of distinct ontogenies, the alveolar lung microenvironment shapes the functions and roles of cells that populate the space. Van de Laar *et al.* showed that all macrophage precursors: yolk-sac macrophages, fetal liver monocytes, and bone marrow monocytes efficiently colonized the alveolar niche and generated functional AMs (Van de Laar et al, 2016). Similarly, it was shown by Gibbings *et al.* that genes in TR-AMs and MO-AMs were tightly correlated (97-99%), and that 20 of 21 transcription factors that are selectively expressed by TR-AMs also displayed an identical gene expression level in MO-AMs (Gibbing et al, 2015). In addition, Lavin *et al.* also observed that adult bone marrow monocytes transplanted into the lungs following irradiation developed enhancers found in TR-AMs (89%-98% resemblance), further confirming the critical role that the alveolar microenvironment plays in establishing AM identity (Lavin et al, 2014).

In healthy individuals, functional AMs eliminate pathogens in a silent manner and inhibit unnecessary lung inflammation. It is estimated that the typical concentration level of bacterial aerosol in homes is 10^3 CFU m^{-3} and 5×10^5 CFU m^{-3} outdoors on a summer day, neither of which would presumably recruit neutrophils in healthy individuals (Pastuszka *et al.*, 1999, Lighthard, 2000). I have determined that the maximum dosage of *S. aureus* that remains under the threshold of neutrophil recruitment to the lungs is approximately 4×10^6 CFU. However, bacterial capture

requires that the AMs are able to crawl and chemotax toward the pathogen. Based on my previous results showing the similar crawling displacements of TR-AMs and MO-AMs, I hypothesized that TR-AMs and MO-AMs would also display similar phagocytic capacities. Indeed, when we introduced 4×10^6 CFU of *S. aureus*-GFP bacteria, a similar percentage of TR-AMs and MO-AMs had phagocytosed the bacteria. This is in line with previous work that suggested no phagocytic advantage between TR-AMs and MO-AMs *ex vivo* (Gibbins et al, 2015). Our data also contributes to previous literature that explored the impact of macrophage ontogeny in other organs. For example, it has been suggested that tissue-resident and monocyte-derived Kupffer cells also display similar biological functions (ie. phagocytosis, response to LPS challenge, and containment of infections) (Beattie et al, 2016; David et al, 2016). Combining the similar crawling behavior and phagocytic capacity, our study suggests that TR-AMs and MO-AMs are seemingly identical during homeostasis at 8-weeks of age.

In our study, we have also examined the behavior of a limited number of mice that were 40-weeks of age and determined that MO-AMs displace larger distances in comparison to TR-AMs. Although this was an interesting observation, there is no stated mechanism for why this occurs. As well, a limited number of experiments were performed to support this result, and further work is required to support this observation. Nevertheless, the data are intriguing and may suggest that with time the function of TR-AMs decreases and are therefore replaced by MO-AMs.

We initially hypothesized that AM depletion would induce rapid monocyte infiltration and populate the alveolar niche. This has been observed in other organs such as the liver, where

monocyte-derived Kupffer cells recruited to the liver following depletion to replace tissue-resident cells (David et al, 2016, Scott et al, 2016). However, in contrast, we noted that TR-AMs repopulated the alveoli following AM depletion. This was an interesting observation and agrees with previous studies that have supported the self-replicative ability of TR-AMs (Hashimoto et al, 2013; Yona et al, 2013). Van de Laar *et al.* also directly compared fetal liver and bone marrow-derived monocytes to colonize the alveolar niche and observed that fetal liver monocytes outcompeted the bone marrow-derived monocytes to occupy 81% of the lung niche (Van de Laar et al, 2016). A possible reason for TR-AMs to quickly occupy the AM niche could be due to a higher proliferative potential in comparison to MO-AMs. Van de Laar *et al.* showed that bone marrow-derived monocytes did not show extensive proliferation capacity in response to GM-CSF *in vitro*, and also expressed lower levels of proliferation-associated genes (Van de Laar et al, 2016).

It is possible that besides MO-AMs and replicating TR-AMs, a third possible source of macrophage replenishment could be the pleural cavity GATA6⁺ macrophages. Our lab has previously shown that cavity macrophages can recruit to injured tissues and perform the roles of resident macrophages (Deniset et al, 2019, Wang and Kubes, 2016). For example, Deniset *et al.* showed that a population of Gata6⁺ macrophages that reside in the pericardial space recruit to the heart following cardiac injury and contribute to cardiac repair (Deniset et al, 2019). These Gata6⁺ macrophages were distinct from cardiac macrophages but lost their Gata6⁺ expression upon recruitment into the heart, suggesting a change in phenotype to adapt to the new microenvironment. Similarly, Wang and Kubes showed that a population of mature Gata6⁺ macrophages from the peritoneal cavity rapidly invade into the liver injury site and contribute to

tissue repair (Wang and Kubes, 2016). This suggests that there is considerable plasticity in mature Gata6⁺ cavity macrophages when they are exposed to another tissue microenvironment. Interestingly, a population of Gata6⁺ macrophages also exist in the pleural cavity which lies in close proximity with the lung. We hypothesized that CLL-induced AM depletion may trigger a migration of these Gata6⁺ macrophages into the alveolar space and become AMs. However, it is worth mentioning that another trainee in the lab using a novel Gata6⁺ reporter mouse did not detect this source of macrophages post-clodronate liposome depletion and replenishment of AMs.

Although it has been shown that monocyte-derived macrophages can acquire an identical transcriptomic profile to tissue-resident macrophages at homeostasis or post-sterile inflammation, the assimilation of monocytes has proven to be a gradual process. For example, following CLL-induced Kupffer cell depletion, monocytes replenished the population but showed delayed acquisition of Kupffer cell functions such as a reduced phagocytic activity for the first 30 days upon replenishment (David et al, 2016). Similarly, it has been shown that recruited monocyte-derived Kupffer cells following diphtheria toxin-induced Kupffer cell depletion only acquired increased gene homology with embryonic-derived Kupffer cells after 30 days (Scott et al, 2016). This indicates that although the genetic profile of monocyte- and embryonic-derived macrophages eventually becomes similar, there is a period of adaptation in the microenvironment where immature macrophages are educated. In the lungs, we have previously shown that upon AM depletion, BALF turbidity significantly increased (Neupane et al, 2020). However, I have shown that by 14 days post-depletion, BALF turbidity had returned to the basal level. Perhaps this is because of the difference in the way in which Kupffer cells versus

AMs were repopulated. However, I did observe defects in AMs after massive depletion including a higher bacteria burden after *S. aureus* infection, suggesting that bacterial clearance was impaired. However, it is interesting that a similar percentage of TR-AM and MO-AM had phagocytosed *S. aureus*, suggesting that both populations of AMs were functioning equally but were unable to fully eradicate the pathogen. This begs the question of whether these artificial macrophage depletion experiments really reflect what happens in a natural turnover where only a few macrophages are replenished at any point in time.

Chapter 4. Training TR-AMs and MO-AMs against IAV infection

4.1 Results

4.1.1 TR-AMs and MO-AMs are both paralyzed after IAV infection

At homeostasis, TR-AMs and MO-AMs are both capable of crawling along the alveoli and phagocytosing bacteria that infiltrate into the alveolar space. However, our lab has previously shown that this crawling behavior is impaired during IAV infection (Neupane et al, 2020). This paralysis increases the severity of secondary bacterial infections as the macrophage cannot get to free bacteria. Although ontogeny of AMs does not appear to determine the behavior and function of TR-AMs and MO-AMs at homeostasis, their responses to a viral infection, and behaviors when homeostasis has shifted are unknown.

To determine if the behavior of TR-AMs and MO-AMs are equally affected by IAV, *Ms4a3^{Cre}Rosa26^{TdT}* mice were infected with 50PFU of IAV. Weight loss was tracked every day or every 2 days, with a maximum weight loss of 20% at day 8, followed by the recovery and return of body weight by day 12 (**Figure 4.1A**). Since it has been previously shown that AMs are paralyzed at 12 days post-IAV infection, the *Ms4a3^{Cre}Rosa26^{TdT}* mice were imaged using IVM at 12 days post-infection to compare the impact of the virus on TR-AMs and MO-AMs. Interestingly, both TR-AMs and MO-AMs were paralyzed at 12 days post-infection in 8-week-old mice. Compared to an average displacement of 30 μ m at homeostasis, both TR-AM and MO-AM crawling was reduced to less than 10 μ m post-IAV infection (**Figure 4.1B, Figure 4.2**). Similarly, at 40-weeks, both TR-AMs and MO-AMs were paralyzed at day 12 post-IAV infection (**Figure 4.1C, Figure 4.2**). Interestingly, infected MO-AMs displaced further than infected TR-AMs, with a maximum displacement of 50 μ m and 20 μ m respectively (**Figure 4.1C,**

Figure 4.2). This indicated that although older TR-AMs and MO-AMs were comparably paralyzed post-IAV infection, MO-AMs were better able to migrate across the alveolar space during flu infection.

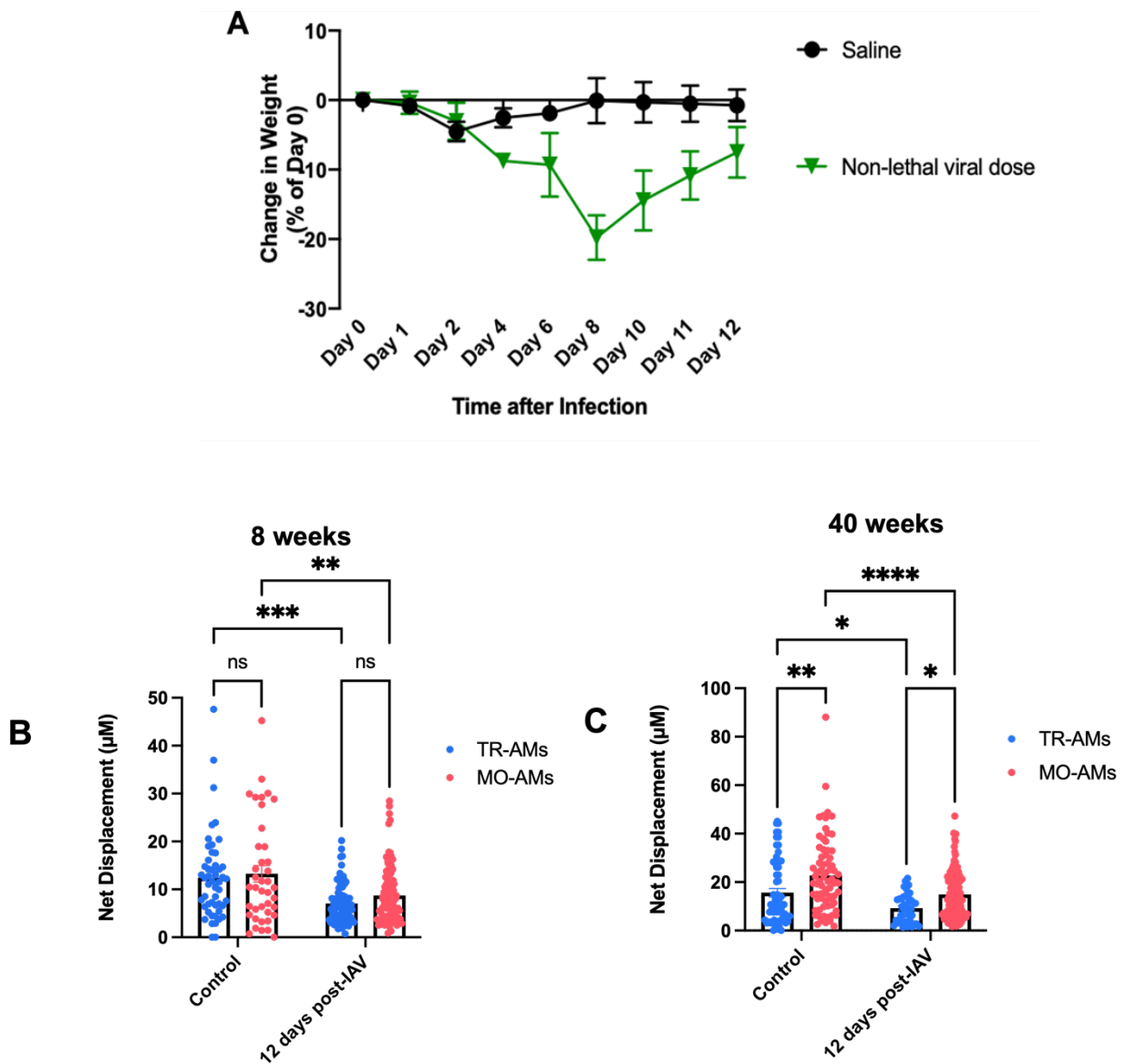


Figure 4. 1. TR-AMs and MO-AMs are both paralyzed at 12 days post-IAV infection in 8- and 40-week mice.

50PFU of IAV or saline was administered through the oropharyngeal route to

Ms4a3^{Cre}Rosa26^{TdT} mice. Weight of saline (black) and infected (green) groups were tracked (A)

over 12 days following IAV infection. 12 days post-infection, IVM was used to track the net

displacement over a 2-hour period. Results show the net displacement of the control saline group (left) and the IAV infected group (right) in TR-AMs (blue) and MO-AMs (red) at 8-weeks (B) and 40-weeks (C). At this time, 3 mice per group were used. 3 FOV were randomly selected per mouse and a maximum of 20 macrophages were selected per FOV. Data are expressed as one data point per macrophage. ns = not significant, * indicates $p < 0.05$, ** indicates $p < 0.01$, *** indicates $p < 0.001$, and **** indicates $p < 0.0001$,

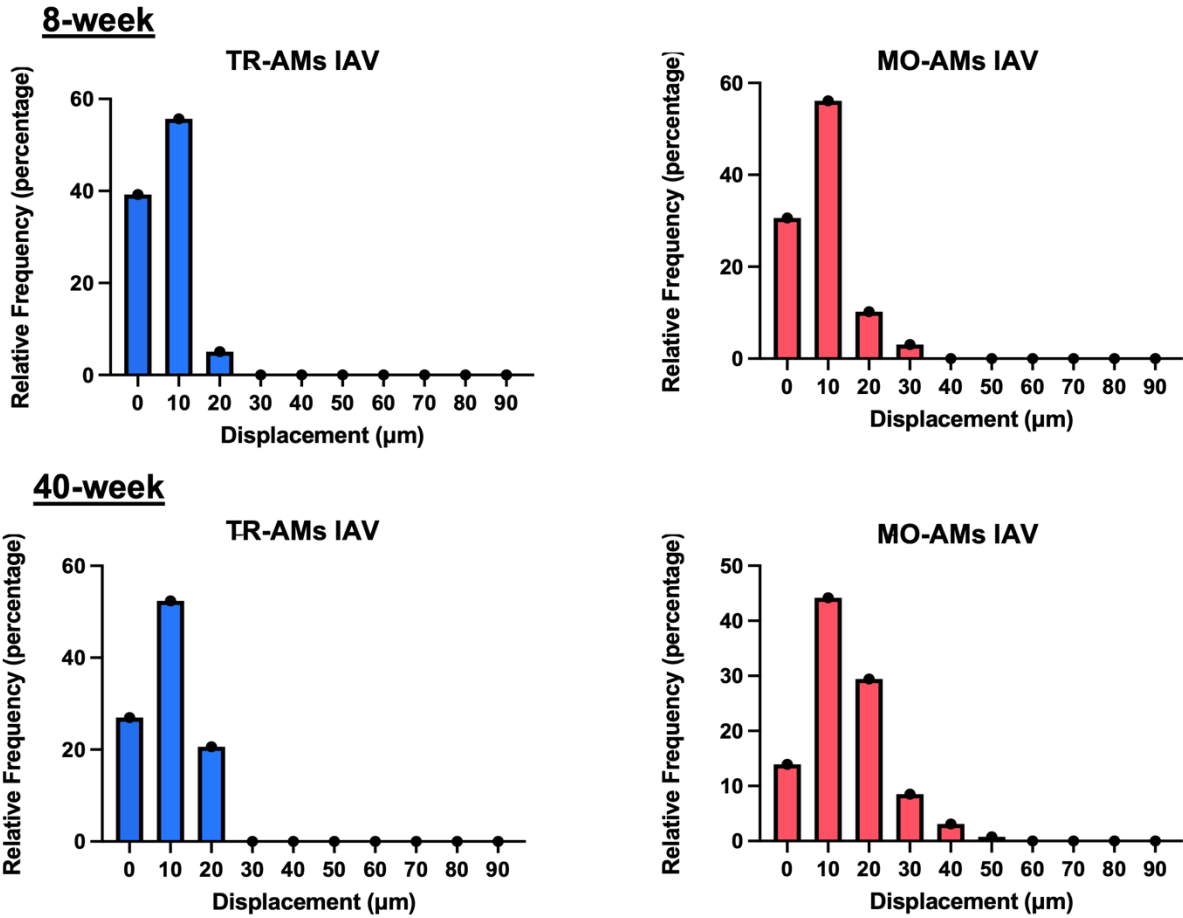


Figure 4. 2. TR-AMs and MO-AMs are similarly paralyzed at 8-weeks but different at 40-weeks after 12 days post-IAV.

IVM was used to visualize TR-AMs and MO-AMs in *Ms4a3^{Cre}Rosa26^{TdI}* mice and displacement in real-time was determined over a 2-hour period. At this time, 3 mice per group were selected. Results show the percentage of TR-AMs (blue) and MO-AMs (red) at distributed displacements of 8- (top) and 40-week (bottom) mice.

4.1.2 β -glucan-induced inflammation resolves 14 days post-administration

Trained immunity has emerged in recent years as memory in the innate immune system and provides non-specific protection. It has been suggested that AMs can also undergo trained immunity. TR-AMs were shown to be trained by adenoviruses where adenovirus-experienced TR-AMs were able to quickly eradicate and reduce the severity of secondary *S. pneumoniae* infection (Yao et al, 2018). Of the available training tools, β -glucan has received considerable attention for its ability to train monocytes to protect against pulmonary *M. tuberculosis* infection (Moorlag et al, 2020). Similarly, it has also been found that β -glucan inhibited the growth of *M. tuberculosis* strain H37Rv in peritoneal macrophages (Hetland and Sandven, 2002). Therefore, we hypothesized that β -glucan can train TR-AMs and/or MO-AMs to prevent IAV-induced paralysis.

As a component of the cell walls in yeast and fungi, it is known that β -glucan induces an inflammatory response in the host (Kutty et al, 2016). To determine if β -glucan truly trains AMs, it is important to determine a timepoint of when β -glucan-induced pulmonary inflammation returns to baseline after β -glucan treatment. To do this, C57BL/6 mice were treated with 1mg β -glucan/200 μ L IP. At 5 days post-treatment, there was a significant increase in the numbers of neutrophils, eosinophils, and monocytes in the lungs, indicating that systemic β -glucan administration has induced lung inflammation (**Figure 4.3**). Neutrophils were identified as CD11b⁺ CD11c⁻ Ly6G⁺ MHCII⁻ SiglecF⁻ Ly6C⁻, eosinophils as CD11b⁺ CD11c⁻ Ly6G⁻ MHCII⁻ SiglecF⁺ Ly6C⁻, and monocytes as CD11b⁺ CD11c⁻ Ly6G⁻ MHCII⁻ SiglecF⁻ Ly6C⁺. At day 14 post-treatment, the number of these inflammatory cells declined and was no longer significantly different from the control group. As well, the total number of AMs remained the same in the

PBS control and 5 and 14 days post- β -glucan treatment groups. This indicated that although lung inflammation was induced, no AM depletion occurred. This also indicated that β -glucan-induced inflammation resolves after 2 weeks, and 14 days was a suitable timepoint to introduce a secondary pathogen to test the functions of AMs.

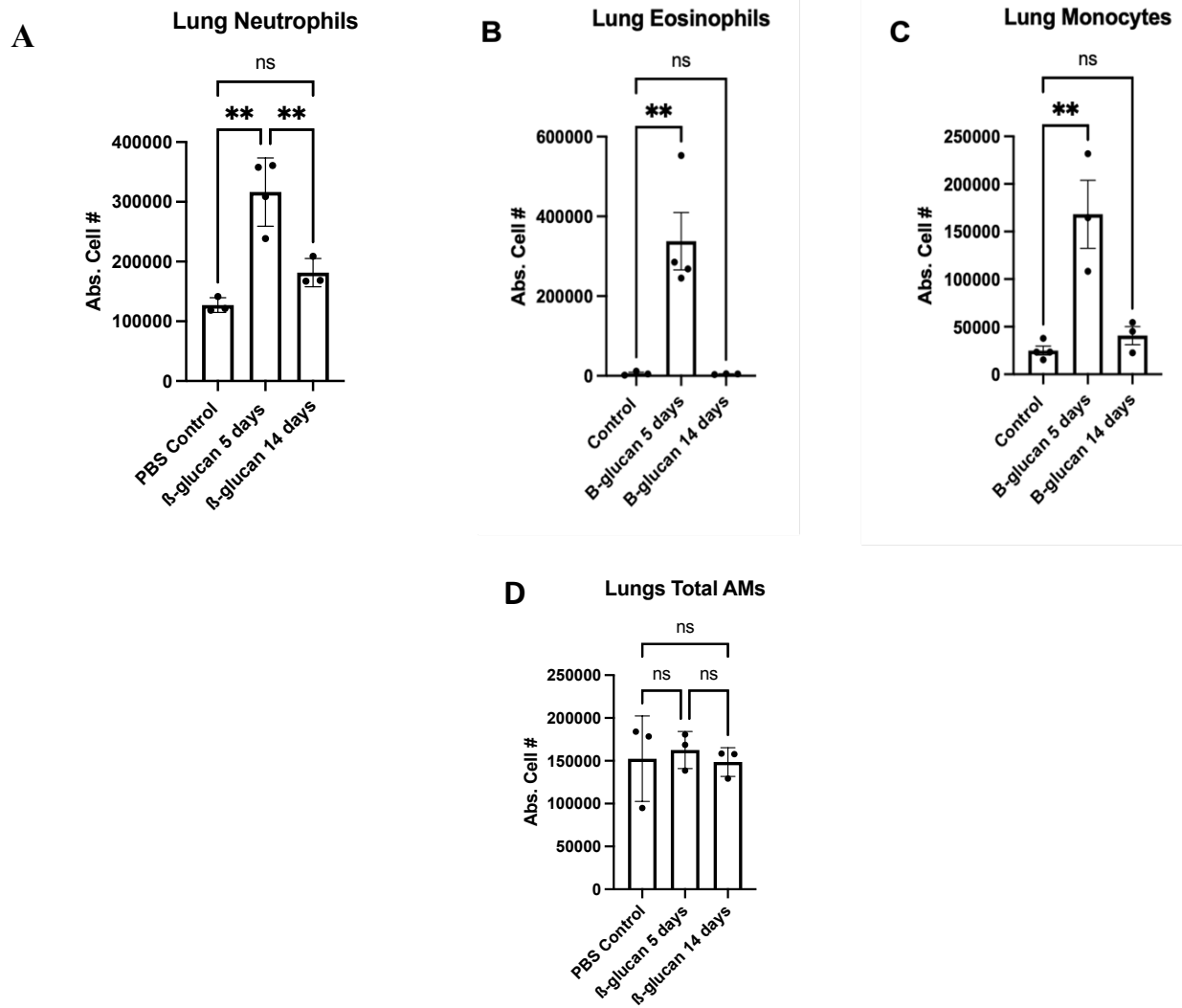


Figure 4. 3. Neutrophils, eosinophils and monocytes in the lung increase at 5 days and drops at 14 days post-β-glucan administration but total AM number remains the same.

1mg of β-glucan was dissolved in 200μL PBS and administered IP to C57BL/6 mice. At 5 days and 14 days post-administration, lungs were collected and processed. Quantification of neutrophils (A), eosinophils (B), monocytes (C), and total AMs (D) was determined through

FACs. Data are expressed as one data point per animal \pm SEM for 4 mice per group. ns = not significant and ** indicates $p < 0.01$.

4.1.3 No turnover of TR-AMs to MO-AMs 14 days after β -glucan treatment

To determine if there is TR-AM to MO-AM turnover after β -glucan administration, 1mg β -glucan/200 μ L was administered IP to *Ms4a3^{Cre}Rosa26^{TdT}* mice. 14 days post-treatment, the BAL and the lungs were collected and processed for FACs. Interestingly, in comparison to the PBS control, the proportion of TR-AMs and MO-AMs did not significantly change after β -glucan treatment (**Figure 4.4A and Figure 4.4B**). This suggests that TR-AM turnover had not occurred at 14 days post-treatment. As well, the total number of AMs in the BAL and lungs remained the same 14 days after PBS and β -glucan treatment, indicating that β -glucan had not induced an AM depletion (**Figure 4.4C and Figure 4.4D**).

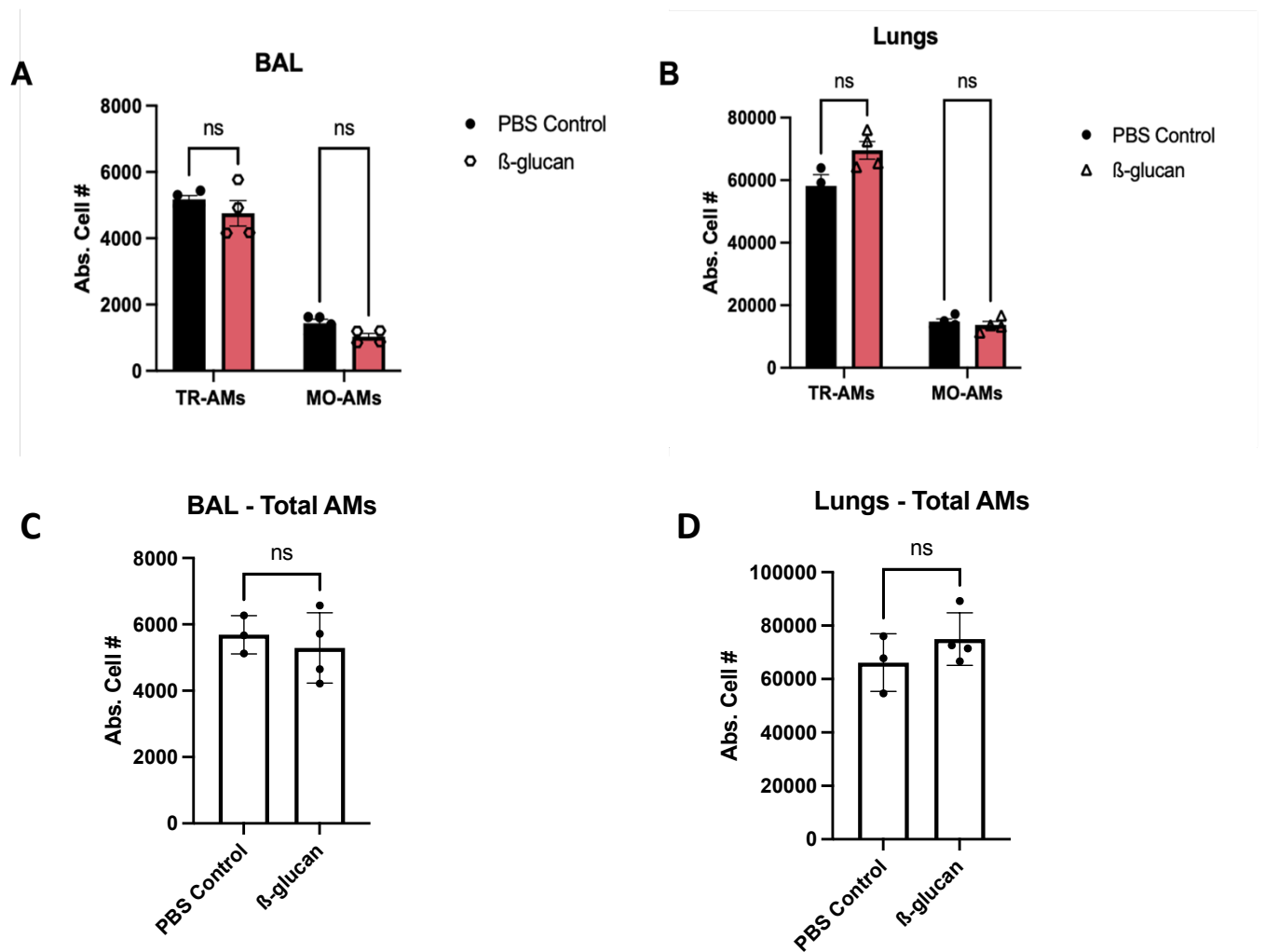


Figure 4. 4. No turnover of TR-AM to MO-AM at 14 days post β -glucan treatment.

1mg of β -glucan was dissolved in 200 μ L PBS and administered IP to *Ms4a3^{Cre}Rosa26^{TdT}* mice.

After 14 days post-administration, BALF (A) and lungs (B) were collected and processed.

Results show the absolute (Abs.) cell number (total number) of TR-AMs (left) and MO-AMs

(right) in PBS (black) and β -glucan (red) treated mice. Total number of AMs are shown in BAL

(C) and lungs (D). Data are expressed as one data point per animal \pm SEM for 3 to 4 mice per

group. ns = not significant.

4.1.4 β -glucan treatment prevents IAV-induced alveolar macrophage paralysis

To determine if β -glucan trained the AMs, mice that have been pre-treated with β -glucan were subsequently challenged with IAV. To do this, PKH26 dye was first administered to the mice through the oropharyngeal route to label all existing AMs. This identified and tracked the macrophages that were present in the alveoli before β -glucan and after β -glucan treatment. 1mg β -glucan/200 μ L was administered IP to C57BL/6 mice. 14 days post-treatment, 50PFU of IAV was administered through the oropharyngeal route. At 12 days post-infection, the mice were imaged using IVM. In comparison to mice that had been infected with IAV in PBS-treated mice, AMs in mice pre-treated with β -glucan displayed a higher displacement post-IAV infection (**Figure 4.5**). Some macrophages recorded a very large displacement of up to 110 μ m, which is higher than the net displacement of homeostatic AMs, demonstrating that not only was IAV-induced paralysis prevented, but displacement had been enhanced with β -glucan. This result showed that β -glucan acted as a potential training tool for AMs and prevented the paralysis caused by IAV infection.

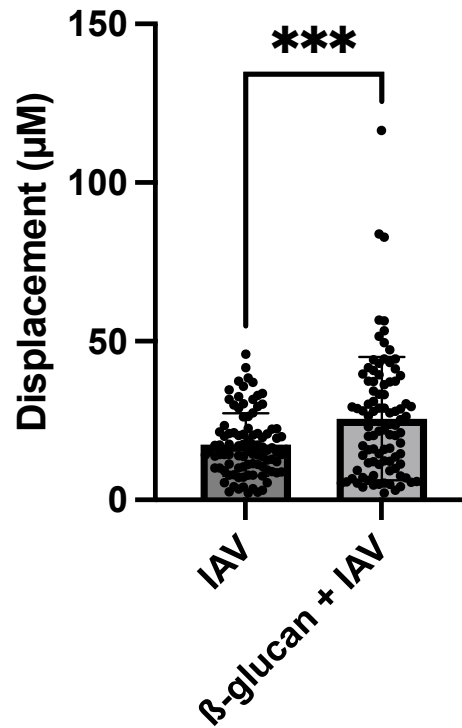


Figure 4. 5. β-glucan treatment prevents the IAV-induced AM paralysis of AMs.

Saline or 1mg of β-glucan was dissolved in 200µL PBS and administered IP to C57BL/6 mice. At 14 days after administration, mice were infected by 50PFU IAV through the oropharyngeal route. 12 days after IAV infection, mice were imaged and displacement of AMs were tracked. Results show the net displacement of the control PBS + IAV group (left) and β-glucan + IAV group (right). At this time, 3 mice per group were selected. 3 FOV were selected per mouse and a maximum of 20 macrophages were selected per FOV. Data are expressed as one data point per macrophage. *** indicates $p < 0.001$.

4.1.5 β -glucan does not alter CD11b⁺ expression in AMs post-IAV infection

CD11b is the alpha subunit that combines with CD18 (β_2 integrin) to form a heterodimer integrin that is expressed on many leukocytes including neutrophils and monocytes. It has been suggested that CD11b is important for neutrophil crawling in the pulmonary vasculature (Yipp et al, 2017). However, in the context of AMs, it has been suggested that this integrin could be involved in AM paralysis. In the most recent study on AMs in our lab, it was reported that AM paralysis at day 12 post-IAV infection was associated with an increase in CD11b expression by the AMs (Neupane et al, 2020). As well, it has been suggested that an increase in susceptibility to secondary bacterial infection following IAV infection was also associated with an increase in CD11b expression by AMs (Sun and Metzger, 2008). Since a new population of CD11b⁺ AMs emerged following IAV infection, it has been suggested that either the CD11b⁺ is a marker of MO-AMs, or an integrin that is up-regulated in activated TR-AMs. Taking this into account, we hypothesized that the CD11b⁺ expression decreases post-IAV infection in pre- β -glucan treated mice.

To determine the expression of the CD11b⁺ marker in AMs, 1 mg β -glucan/200uL was administered IP to C57BL/6 mice. 14 days later, 50PFU of IAV was used to infect the mice and FACs was conducted 12 days post-infection. Using an identical AM gating strategy to the one described above, the MFI of CD11b was identified and compared. Interestingly, in comparison to the PBS-IAV control group, the β -glucan -IAV group had a similar CD11b MFI (**Figure 4.6**). This indicated that although IAV-induced AM paralysis was prevented by β -glucan, CD11b remained similar and therefore is not associated with the decreased movement of AMs post-IAV infection nor the increase in movement of AMs in pre- β -glucan treated mice.

Lungs MFI CD11b+ in all AMs

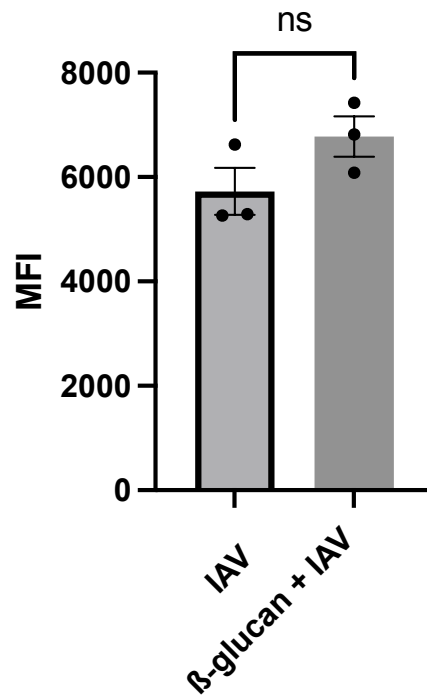


Figure 4. 6. Median Fluorescent Intensity (MFI) of CD11b is not different in AMs after IAV infection in PBS and β -glucan pre-treated conditions.

Saline or 1mg of β -glucan was dissolved in 200 μ L PBS and administered IP to C57BL/6 mice.

14 days after administration, mice were infected by 50PFU of IAV through the oropharyngeal route. 12 days after IAV infection, lungs were collected and processed. Results show the MFI of CD11b in AMs in the control PBS + IAV group (left) and β -glucan + IAV group (right). Data are expressed as one data point per animal \pm SEM for 3 mice per group. ns = not significant.

4.1.6 TR-AM and MO-AM paralysis post-IAV infection have both been restored with prior treatment with β -glucan.

Based on the results in 4.1.4 where we observed an increase in the net displacement of AMs post-IAV infection with prior β -glucan treatment, this experiment was repeated in *Ms4a3^{Cre}Rosa26^{TdT}* mice to determine whether TR-AMs or MO-AMs were trained. To do this, CellVue Claret dye was administered through the oropharyngeal route to label all macrophages in the alveolar space. 5 days later, β -glucan was administered IP to one group of mice, and PBS was administered to the control group. 14 days post- β -glucan/PBS treatment, 50PFU of IAV was administered through the oropharyngeal route to both groups of mice. At 12 days post-infection, both groups of mice were imaged over a 2-hour period through IVM. The net displacement of TR-AMs and MO-AMs were then analyzed through the Imaris software. Like results described in 4.1.4, AMs were paralyzed in the PBS+IAV group, and were observed to occur in both TR-AMs and MO-AMs. However, in the β -glucan group, it was noted that both TR-AMs and MO-AMs displaced great distances (**Figure 4.7**). This suggests that prior treatment with β -glucan had prevented the IAV-induced macrophage paralysis. This result also suggests that both TR-AMs and MO-AMs were trained immunity candidates.

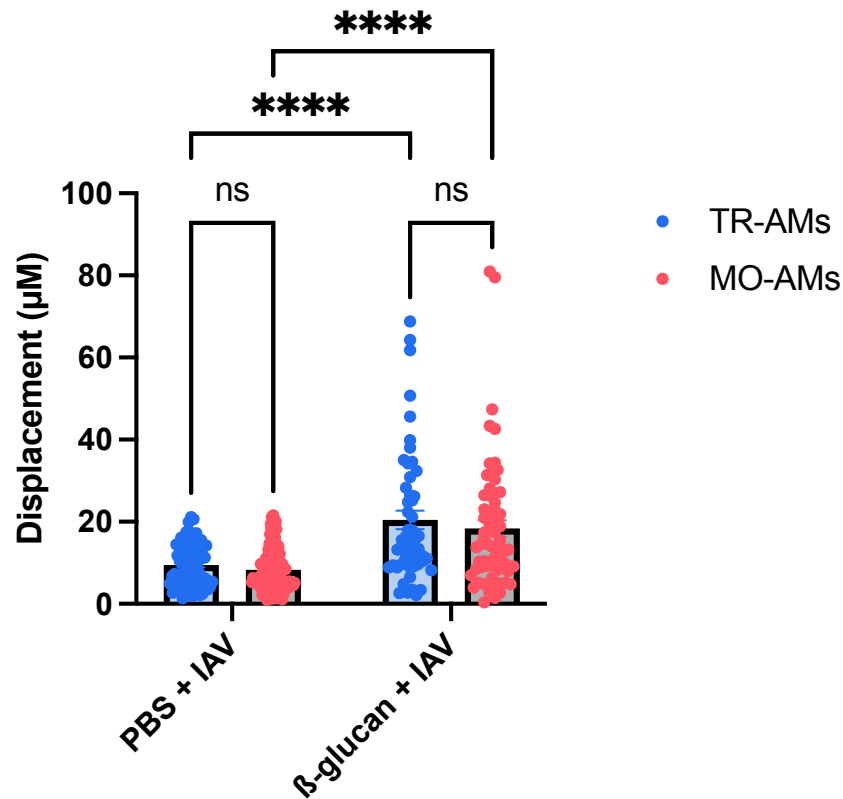


Figure 4. 7. The motility of TR-AMs and MO-AMs are restored at 12 days post-IAV infection after prior treatment with β-glucan.

Saline or 1mg of β-glucan was dissolved in 200µL PBS and administered IP to

Ms4a3^{Cre}Rosa26^{TdT} mice. 14 days after administration, mice were then infected by 50PFU of

IAV through the oropharyngeal route. 12 days after IAV infection, mice were imaged and net

displacements of TR-AM and MO-AMs were tracked. Results show the net displacement of the

control PBS + IAV group (left) and β-glucan + IAV group (right). 3 FOV were selected per

mouse and a maximum of 20 macrophages were selected per FOV. Data are expressed as one

data point per macrophage. ns = not significant. **** indicates $p < 0.0001$.

4.2 Discussion

In this study, I showed that both TR-AMs and MO-AMs were paralyzed by IAV infection at 8-weeks and at 40-weeks. Using β -glucan, a common trained immunity inducing tool, I identified no TR-AM to MO-AM turnover following β -glucan-induced inflammation, but interestingly, I observed that β -glucan prevented IAV infection-induced TR-AM and MO-AM paralysis.

Several studies have reported the phenotypical changes that occur in AMs during IAV infection. *Sun and Metzger* showed that IAV infection reduces the phagocytic capacity of AMs to pneumococcal infection, resulting in reduced bacterial clearance and increased mortality (Sun and Metzger, 2008). Mechanistically, this phagocytic impairment was associated with an increase of IFN γ production during IAV infection which was suggested to downregulate the MARCO phagocytic receptor (Sun and Metzger, 2008). In agreement, Califano *et al.* also demonstrated that IAV increased the susceptibility and mortality to secondary *S. pneumoniae* infection despite a retention of AM numbers during IAV infection (Califano et al, 2018). Recently, our lab provided an additional explanation for the impaired secondary bacterial capture post-IAV infection. Using IVM, Neupane *et al.* showed that IAV induces AM paralysis and inhibition of chemotaxis towards inhaled bacteria (*P. aeruginosa* and *S. aureus*). In my project, I showed that both TR-AMs and MO-AMs are paralyzed during IAV infection. This result supports the notion that instead of ontogeny, the alveolar microenvironment may dictate the behavior of resident TR-AMs and MO-AMs.

It has been suggested that IAV infection induced phagocytic impairment only in TR-AMs (Roquilly et al, 2020). My finding does not agree with this claim. It should be noted that Roquilly *et al.* used a combination of intravenous administration of anti-CD45 and IT administration of PKH26 to distinguish MO-AMs and TR-AMs respectively. This method, due to the limitations of persistence of antibody labelling and the possibility MO-AMs taking up PKH26 from dead TR-AMs, may lead to mislabeling of the two macrophages. Although a bacterial capture experiment to compare the phagocytic ability of TR-AMs and MO-AMs during IAV infection was not conducted in my study, I hypothesize that both populations will exhibit impaired phagocytic capacity based on their similar paralyzed state.

I showed that although MO-AMs displaced farther than TR-AMs at homeostasis at 40-weeks of age, both macrophage populations were still paralyzed by the IAV. As a limited number of experiments were conducted of mice at this age, how aging affects the severity and IAV-induced pathogenesis remains to be explored. It would also be worthwhile to investigate the longevity of this paralysis and compare when TR-AMs and MO-AMs restore their behavior post-IAV infection. As well, it would also be an area of interest to compare the production of cytokines secreted by TR-AMs and MO-AMs against IAV infection at 8- and 40-weeks of age. Due to the higher proportion of MO-AMs, it would be interesting to compare the extent of lymphocyte recruitment as monocytes have been shown to interact closely with CD8⁺ T-cells during IAV infection (Schmit et al, 2022; Yao et al, 2018).

I noted that β -glucan-induced lung inflammation characterized by elevations of neutrophils, monocytes, and eosinophils that resolve after 14 days. Interestingly, TR-AM and

MO-AM ratio was not significantly different at 14 days post- β -glucan treatment. This was surprising as β -glucan has been shown to increase the number of monocytes in the lungs (Moorlag et al, 2018). However, a different approach was used by Moorlag *et al.* who administered 2 doses of β -glucan and reported this infiltration at 3 days post-treatment. A possible explanation for the lack of turnover could be due to the intact AM number throughout β -glucan treatment. Therefore, there is no need for MO-AMs to replace TR-AMs as the alveolar niche remains inaccessible and resident macrophages remain able to self-maintain (Guillams et al, 2013).

Recognized as a common training tool, β -glucan has emerged for modulating the metabolism and epigenetic landscape of innate immune cells. Consistent with previous studies that have suggested the protective effects of β -glucan against bacterial and viral infections in the upper and lower respiratory tract, our study also suggests that β -glucan can protect AMs from IAV-induced paralysis. This observation may also suggest a mitigated impact on TR-AMs and MO-AMs and an increased ability to eliminate secondary bacterial infections. In the human diet, β -glucan is commonly found in oats, wheat, barley, and certain mushrooms, thus making this polysaccharide a common reagent in our diets. Further investigations on the effects that β -glucan have on innate immune cells is needed to unveil the beneficial effects of β -glucan addition to our diet.

Chapter 5. Limitations and future directions

5.1. Limitations and future directions

My project has a number of limitations. First, I acknowledge the limited number of experiments conducted for mice at 40 weeks of age. Only 6 mice were available to study the homeostatic behavior of TR-AMs and MO-AMs, and only 7 mice were available to study TR-AM and MO-AM behavior post-IAV infection. Therefore, results highlighted for this age category remain preliminary and further experiments are required. From my results in Chapter 3, I have noted that MO-AMs at 40-weeks displace farther than TR-AMs at homeostasis. To study if this increase in motility is associated with primary function, it would be of interest to infect with *S. aureus* and explore their phagocytic abilities. Moreover, I observed more MO-AMs than TR-AMs at 40-weeks versus 8-weeks. Since the former has been implicated with greater inflammation, it would be worth measuring pro-inflammatory cytokines and tissue injury at the peak of infection between the two age groups (Aegerter et al, 2020; Mould et al, 2016; Li et al, 2022; Schmit et al, 2022).

In my experiments using CLL to deplete AMs, I have noticed a higher bacteria burden in the lungs 14 days post-administration of *S. aureus*. However, only ~60% of the total AMs have recovered from depletion. Therefore, it is unknown whether the increase in free floating bacteria is a result of malfunctioning AMs or lack of AMs. For future experiments, it would be imperative to determine a reproducible timepoint where all AM numbers have returned to baseline levels (possibly 30 days post-CLL treatment). This would determine if replenishing new AMs after artificial depletion with chlodronate manifests with functions of mature resident AMs. Interestingly, I noted similar phagocytic abilities between new TR-AMs and MO-AMs post-CLL

administration, but it was about 30% less than what is observed without CLL pre-treatment. This could account for the comparatively high bacteria burden, or it could be due to a lack of bacteria killing by macrophages. It has been shown that *S. aureus* can replicate and survive inside Kupffer cells, hindering bacterial elimination (Surewaard et al, 2016). Therefore, it would also be of interest to visualize and quantify the bacteria inside the TR-AMs and MO-AMs at 14 days post-CLL administration. Moreover, although CLL is widely used as a phagocyte depletion method, the adverse effects of this drug have been illustrated in recent literature. For example, it was demonstrated that CLL increased pro-inflammatory cytokine levels and damaged blood vessel integrity in the brain (Han et al, 2019). Therefore, despite the common usage of CLL, it would be important to explore alternative means of AM depletion. This includes using the *Csf2r*^{-/-} mouse model which lack AMs but can be successfully adoptively transferred with TR-AMs or MO-AMs (Subramanian et al, 2022). It would be interesting to isolate the TR-AMs and MO-AMs at 14 days post-CLL treatment and transfer these cells into the *Csf2r*^{-/-} model to determine whether the artificial procedure begets different results.

Although β -glucan seems to have trained both TR-AMs and MO-AMs equally well, I did not consider the possibility that existing MO-AMs could have been replaced by new MO-AMs following infection that would be devoid of CellVue Claret dye leaving the newly recruited MO-AMs induced by IAV infection unlabeled and impossible to identify. For future experiments, using the *Ms4a3*^{CreERT}TdT mouse model, which labels monocyte progenitors upon administration of tamoxifen, would allow labelling of newly recruited MO-AMs. Tamoxifen would be administered prior to IAV infection but after β -glucan treatment.

Our study has not explored the mechanism of how β -glucan prevented IAV-induced AM paralysis. Previously, our lab has suggested the association of AM paralysis with the increase of the IFN γ during IAV infection. Therefore, we hypothesized that β -glucan either 1) reduces the level of IFN γ production or 2) inhibits the downstream IFN γ signalling pathway on AMs. Further experiments are required to determine the source of IFN γ production as well as the level of IFN γ following β -glucan administration. Since β -glucan expands myelopoiesis of monocyte progenitors which are rapidly recruited to injured tissues, this could mean that β -glucan-induced early monocyte recruitment into lungs during IAV infection, which could be affecting macrophage function perhaps by reducing viral dissemination and decreasing IFN γ production at the peak of infection as has been postulated by others (Moorlag et al, 2018).

Trained immunity is characterized by epigenetic remodeling, but my study has not explored any potential epigenome changes induced by β -glucan. For future experiments, I propose using a single-cell assay for Transposase-Accessible Chromatin using sequencing (scATAC-seq) to compare the chromatin structure of TR-AMs and MO-AMs prior to and post- β -glucan treatment to determine if training alters the epigenome. Next, to determine if epigenetic changes are a cause in preventing TR-AM and MO-AM paralysis, it would be important to reverse epigenetic changes using epidrugs, such as histone methyltransferase inhibitors, selected based on our scATAC-seq data, to reverse or block AM reprogramming with β -glucan. This would provide further support to establish that trained immunity prevented IAV-induced macrophage paralysis.

MO-AM recruitment during IAV has been observed in previous studies but the impact of this recruitment could be detrimental. For example, it has been proposed by multiple studies that monocyte recruitment during IAV infection exacerbates the infection and promotes lung injury (Li et al, 2022, Schmit et al, 2022, Coates et al, 2018; Mould et al, 2016). As pro-inflammatory cells, these authors have suggested an increase of MO-AMs contributes towards creating an inflammatory microenvironment. In our study, we did not quantify inflammation, viral load or tissue injury after IAV infection with and without β -glucan treatment. Moreover, our study suggests that IAV-induced paralysis can be prevented in both TR-AMs and MO-AMs by β -glucan. To test if the training of TR-AMs can occur independently of effects on monocyte progenitors and monocytes, it would be interesting to inhibit the recruitment of monocytes. Therefore, experiments using CCR2KO mouse strain would be interesting. This approach would determine if β -glucan training can occur independently of monocyte recruitment to the lungs and if tissue-resident macrophages can also be trained by β -glucan.

5.2. Summary

My study has shown that AMs are slowly turned over as the mouse ages. I also found that as the mouse ages from 8- to 40-weeks, both TR-AMs and MO-AMs improve on crawling and perhaps eradicating pathogens. My work also shows for the first time that both TR-AMs and MO-AMs are paralyzed by flu and that β -glucan, a training tool that can prevent this paralysis in both subsets of macrophages. This does not exclude the possibility that it is the monocyte progenitors that are actually trained and migrate into the tissue to then modify TR-AM and MO-AM function, but it does unveil that β -glucan can either indirectly or directly affect resident macrophage populations. Finally, while I saw very few differences between MO-AMs and TR-AMs as they naturally turnover, but I did see some significant deficiencies when the AMs were

depleted with CLL raising the possibility that depleting all AMs en masse artificially may not reflect alveolar macrophage turnover during normal physiologic conditions.

References

- Aegerter H, Kulikauskaite J, Crotta S, Patel H, Kelly G, et al. Influenza-induced monocyte-derived alveolar macrophages confer prolonged antibacterial protection. *Nat Immunol*. 2020;21(2):145-157.
- Aldridge J, Moseley C, Boltz D, Negovetich N, Reynolds C, et al. TNF/iNOS-producing dendritic cells are the necessary evil of lethal influenza virus infection. *Proc. Natl. Acad. Sci*. 2009;106:5306–5311.
- Al tuwajiri A, Mahmoud A, Al mofleh I, Al khuwaitir S. Effect of glucan on *Leishmania major* infection in BALB/c mice. *J Med. Microbiol*. 1987;23(4):363–365.
- Ajami B, Bennett J, Krieger C, et al. Local self-renewal can sustain CNS microglia maintenance and function throughout adult life. *Nat Neurosci*. 2007;10:1538–154.
- Arafa E, Shenoy A, Barker K, Etesami N, Martin I, et al. Recruitment and training of alveolar macrophages after pneumococcal pneumonia. *JCI Insight*. 2022;7(5):e150239.
- Arredouani M, Kasran A, Vanoirbeek J, Berger F, Baumann H, Ceuppens J. Haptoglobin dampens endotoxin-induced inflammatory effects both in vitro and in vivo. *Immunology*. 2005;114(2):263-71.
- Arts R, Moorlag S, Novakovic B, Li Y, Wang SY, et al. BCG Vaccination Protects against Experimental Viral Infection in Humans through the Induction of Cytokines Associated with Trained Immunity. *Cell Host Microbe*. 2018;23(1):89-100.e5.
- Auffray C, Fogg D, Garfa M, Elain G, Join-Lambert O, et al. Monitoring of blood vessels and tissues by a population of monocytes with patrolling behavior. *Science*. 2007;317(5838):666-70.
- Bain C, Bravo-Blas A, Scott C, Perdiguero E, Geissmann F et al. Constant replenishment from circulating monocytes maintains the macrophage pool in the intestine of adult mice. *Nat Immunol*. 2014 Oct;15(10):929-937.
- Baker A, Malur A, Barna B, Ghosh S, Kavuru M, et al. Targeted PPAR $\{\gamma\}$ deficiency in alveolar macrophages disrupts surfactant catabolism. *J Lipid Res*. 2010;51(6):1325-31.
- Beattie L, Sawtell A, Mann J, Frame TCM, et al. Bone marrow-derived and resident liver macrophages display unique transcriptomic signatures but similar biological functions. *J Hepatol*. 2016 Oct;65(4):758-768.
- Bistoni F, Vecchiarelli A, Cenci E, Puccetti P, Marconi P, et al. Evidence for macrophage-mediated protection against lethal *Candida albicans* infection. *Infect Immun*. 1986;51(2):668-74.
- Bonfield T, Panuska J, Konstan M, Hilliard K, Hilliard J, et al. Inflammatory cytokines in cystic fibrosis lungs. *Am J Respir Crit Care Med*. 1995;152(6 Pt 1):2111-8.

Bousquet M, Escoula L, Pipy B, Bessières MH, Chavant L, et al. Augmentation de la résistance des souris à *Toxoplasma gondii* par deux polysaccharides beta 1-3, beta 1-6 (le PSAT et le Scléroglycane). *Ann Parasitol Hum Comp*. 1988;63(6):398-409.

Brandes M, Klauschen F, Kuchen S, Germain RN. A systems analysis identifies a feedforward inflammatory circuit leading to lethal influenza infection. *Cell*. 2013;154(1):197-212.

Brandt J, Mandiga P. Histology, Alveolar Cells. 2022.

Brinkmann V, Reichard U, Goosman C, Fauler B, Uhlemann Y, et al. Neutrophil Extracellular Traps Kill Bacteria. *Science*. 2004;303,1532-1535.

Brown G, Taylor P, Reid D, Willment J, Williams D, et al. Dectin-1 is a major beta-glucan receptor on macrophages. *J Exp Med*. 2002;196(3):407-12.

Buscher K, Marcovecchio P, Hedrick C, Ley K. Patrolling Mechanics of Non-Classical Monocytes in Vascular Inflammation. *Front Cardiovasc Med*. 2017;4:80.

Byrne A, Powell J, O'Sullivan B, Ogger P, Hoffland A, et al. Dynamics of human monocytes and airway macrophages during healthy aging and after transplant. *J Exp Med*. 2020;217(3):e20191236.

Califano D, Furuya Y, Metzger D. Effects of Influenza on Alveolar Macrophage Viability Are Dependent on Mouse Genetic Strain. *J Immunol*. 2018;201(1):134-144.

Cardani A, Boulton A, Kim T, Braciale T. Alveolar Macrophages Prevent Lethal Influenza Pneumonia By Inhibiting Infection Of Type-1 Alveolar Epithelial Cells. *PLoS Pathog*. 2017;13(1):e1006140.

Carey B, Trapnell B. The molecular basis of pulmonary alveolar proteinosis. *Clin Immunol*. 2010;135(2):223-35.

Carlin L, Stamatiades E, Auffray C, Hanna RN, Glover L, et al. Nr4a1-dependent Ly6C(low) monocytes monitor endothelial cells and orchestrate their disposal. *Cell*. 2013;153(2):362-75.

Cecchini M, Dominguez M, Mocci S, Wetterwald A, Felix R, et al. Role of colony stimulating factor-1 in the establishment and regulation of tissue macrophages during postnatal development of the mouse. *Development*. 1994;120(6):1357-72.

Chronos Z, Sever-Chronos Z, Shepherd V. Pulmonary surfactant: an immunological perspective. *Cell Physiol Biochem*. 2010;25(1):13-26.

Clausen B, Burkhardt C, Reith W, et al. Conditional gene targeting in macrophages and granulocytes using LysMcre mice. *Transgenic Res*. 1999;8, 265-277.

Dai X, Zong X, Sylvestre V, Stanley E. Incomplete restoration of colony-stimulating factor 1 (CSF-1) function in CSF-1-deficient *Csf1op/Csf1op* mice by transgenic expression of cell surface CSF-1. *Blood* 2004;103:1114–1123.

David B, Rezende R, Antunes M, Santos M, Freitas Lopes M, et al. Combination of Mass Cytometry and Imaging Analysis Reveals Origin, Location, and Functional Repopulation of Liver Myeloid Cells in Mice. *Gastroenterology*. 2016;151(6):1176-1191.

Davies L, Rosas M, Jenkins S, Liao C, Scurr M, Brombacher F, et al. Distinct bone marrow-derived and tissue-resident macrophage lineages proliferate at key stages during inflammation. *Nat Commun*. 2013;4:1886.

Dawson T, Beck M, Kuziel W, Henderson F, Maeda N. Contrasting effects of CCR5 and CCR2 deficiency in the pulmonary inflammatory response to influenza A virus. *Am J Pathol*. 2000;156(6):1951-9.

Deniset J, Belke D, Lee W, Jorch S, Deppermann C, et al. *Gata6*⁺Pericardial Cavity Macrophages Relocate to the Injured Heart and Prevent Cardiac Fibrosis. *Immunity*. 2019;16;51(1):131-140.e5.

Divangahi M, Aaby P, Khader S et al. Trained immunity, tolerance, priming and differentiation: distinct immunological processes. *Nat Immunol*. 2021;22, 2–6.

Epelman S, Lavine K, Randolph G. Origin and functions of tissue macrophages. *Immunity*. 2014;41(1):21-35.

Evren E, Ringqvist E, Tripathi KP, Sleiers N, Rives IC, et al. Distinct developmental pathways from blood monocytes generate human lung macrophage diversity. *Immunity*. 2021;9;54(2):259-275.e7.

Fernandez S, Jose P, Avdiushko M, Kaplan A, Cohen D. Inhibition of IL-10 receptor function in alveolar macrophages by Toll-like receptor agonists. *J Immunol*. 2004;172(4):2613-20.

Fogg D, Sibon C, Miled C, Jung S, Aucouturier P, et al. A clonogenic bone marrow progenitor specific for macrophages and dendritic cells. *Science*. 2006;311:83–87.

Gantner B, Simmons R, Canavera S, Akira S, Underhill D. Collaborative induction of inflammatory responses by dectin-1 and Toll-like receptor 2. *J Exp Med*. 2003;5;197(9):1107-17.

Gardai S, Xiao Y, Dickinson M, Nick J, Voelker D, et al. By binding SIRP α or calreticulin/CD91, lung collectins act as dual function surveillance molecules to suppress or enhance inflammation. *Cell*. 2003;115(1):13-23.

Gautier E, Shay T, Miller J. et al. Gene-expression profiles and transcriptional regulatory pathways that underlie the identity and diversity of mouse tissue macrophages. *Nat Immunol*. 2012;13:1118–1128.

- Geissmann F, Jung S, Littman DR. Blood monocytes consist of two principal subsets with distinct migratory properties. *Immunity*. 2003;19(1):71-82.
- Geissmann F, Manz M, Jung S, Sieweke M, Merad M, et al. Development of monocytes, macrophages, and dendritic cells. *Science*. 2010;327(5966):656-61.
- Ghoneim H, Thomas P, McCullers J. Depletion of alveolar macrophages during influenza infection facilitates bacterial superinfections. *J. Immunol*. 2013;191:1250–1259.
- Gill J, Sheng Z, Ely S, Guinee D, Beasley M, et al. Pulmonary pathologic findings of fatal 2009 pandemic influenza A/H1N1 viral infections. *Arch Pathol Lab Med*. 2010;134(2):235-43.
- Gibbins S, Goyal R, Desch A, Leach S, Prabagar M, et al. Transcriptome analysis highlights the conserved difference between embryonic and postnatal-derived alveolar macrophages. *Blood*. 2015;126(11):1357-66.
- Ginhoux F, Williams M. Tissue-Resident Macrophage Ontogeny and Homeostasis. *Immunity*. 2016;44(3):439-449.
- Godleski J, Brain J. The origin of alveolar macrophages in mouse radiation chimeras. *J Exp Med*. 1972;136(3):630-43.
- Goss V, Hunt A, Postle A. Regulation of lung surfactant phospholipid synthesis and metabolism. *Biochim Biophys Acta*. 2013;1831(2):448-58.
- Gregory P, Schmid A, Zavari M, Lui L, Berger S, et al. Absence of Gcn5 HAT activity defines a novel state in the opening of chromatin at the PHO5 promoter in yeast. *Mol. Cell*. 1998;1:495–505.
- Williams M, De Kleer I, Henri S, Post S, Vanhoutte L, et al. Alveolar macrophages develop from fetal monocytes that differentiate into long-lived cells in the first week of life via GM-CSF. *J Exp Med*. 2013;210(10):1977-92.
- Guillon A, Arafa E, Barker K, Belkina A, Martin I, et al. Pneumonia recovery reprograms the alveolar macrophage pool. *JCI Insight*. 2020;5(4):e133042.
- Gupta S, Kim S, Artis S, Molfese D, Schumacher A, et al. Histone methylation regulates memory formation. *J Neurosci*. 2010;30(10):3589-99.
- Haczku A. Protective role of the lung collectins surfactant protein A and surfactant protein D in airway inflammation. *J Allergy Clin Immunol*. 2008;122(5):861-79.
- Han X, Li Q, Lan X, El-Mufti L, Ren H, et al. Microglial Depletion with Clodronate Liposomes Increases Pro-inflammatory Cytokine Levels, Induces Astrocyte Activation, and Damages Blood Vessel Integrity. *Mol Neurobiol*. 2019;56(9):6184-6196.

Hashimoto D, Chow A, Noizat C, Teo P, Beasley MB, et al. Tissue-resident macrophages self-maintain locally throughout adult life with minimal contribution from circulating monocytes. *Immunity*. 2013;38(4):792-804.

Headley M, Bins A, Nip A, Roberts E, Looney M, et al. Visualization of immediate immune responses to pioneer metastatic cells in the lung. *Nature*. 2016;531(7595):513-7.

Hetland G, Sandven P. beta-1,3-Glucan reduces growth of *Mycobacterium tuberculosis* in macrophage cultures. *FEMS Immunol Med Microbiol*. 2002;33(1):41-5.

Hettinger J, Richards D, Hansson J, Barra M, Joschko AC, et al. Origin of monocytes and macrophages in a committed progenitor. *Nat Immunol*. 2013;14:821-830.

Higashi K, Naito M, Takeya M, Ando M, Araki S, et al. Ontogenetic development, differentiation, and phenotypic expression of macrophages in fetal rat lungs. *J. Leukoc. Biol*. 1992;51:444-454.

Hoeffel G, Wang Y, Greter M, See P, Teo P, et al. Adult Langerhans cells derive predominantly from embryonic fetal liver monocytes with a minor contribution of yolk-sac-derived macrophages. *J Exp Med*. 2012;209(6):1167-81.

Hussell T, Bell T. Alveolar macrophages: plasticity in a tissue-specific context. *Nat Rev Immunol*. 2014;14(2):81-93.

Jenkins S, Ruckerl D, Cook P, Jones L, Finkelman F, et al. Local macrophage proliferation, rather than recruitment from the blood, is a signature of TH2 inflammation. *Science*. 2011;332:1284-1288.

Jeyanathan M, Afkhami S, Smaill F, et al. Immunological considerations for COVID-19 vaccine strategies. *Nat Rev Immunol*. 2020:615-632.

Jha A, Huang S, Sergushichev A, Lampropoulou V, Ivanova Y, et al. Network integration of parallel metabolic and transcriptional data reveals metabolic modules that regulate macrophage polarization. *Immunity*. 2015;42(3):419-30.

Kim H, Lee Y, Lee K, Kim H, Cho S, et al. Alveolar macrophages are indispensable for controlling influenza viruses in lungs of pigs. *J Virol*. 2008;82(9):4265-74.

Kitur K, Wachtel S, Brown A, Wickersham M, Paulino F, et al. Necroptosis Promotes *Staphylococcus aureus* Clearance by Inhibiting Excessive Inflammatory Signaling. *Cell Rep*. 2016;16(8):2219-2230.

Kleinnijenhuis J, Quintin J, Preijers F, Joosten LA, Ifrim DC, et al. Bacille Calmette-Guerin induces NOD2-dependent nonspecific protection from re-infection via epigenetic reprogramming of monocytes. *Proc Natl Acad Sci*. 2012;109(43):17537-42.

- Knudsen L, Ochs M. The micromechanics of lung alveoli: structure and function of surfactant and tissue components. *Histochem Cell Biol.* 2018;150(6):661-676.
- Kogan G, Pajtinka M, Babincova M, Miadokova E, Rauko P, et al. Yeast cell wall polysaccharides as antioxidants and antimutagens: Can they fight cancer? *Neoplasma.* 2008;55:387-393.
- Kokoshis P et al. Increased Resistance to Staphylococcus aureus Infection and Enhancement in Serum Lysozyme Activity by Glucan. *Science.* 1978;199:1340-1342.
- Kourtis A, Hatfield K, Baggs J, Mu Y, See I, et al. Vital Signs: Epidemiology and Recent Trends in Methicillin-Resistant and in Methicillin-Susceptible Staphylococcus aureus Bloodstream Infections. *Morb Mortal Wkly Rep.* 2019;68(9):214-219.
- Kratofil R, Kubes P, Deniset J. Monocyte Conversion During Inflammation and Injury. *Arterioscler Thromb Vasc Biol.* 2017;37(1):35-42.
- Kutty G, Davis A, Ferreyra G, Qiu J, Huang da W, et al. β -Glucans Are Masked but Contribute to Pulmonary Inflammation During Pneumocystis Pneumonia. *J Infect Dis.* 2016;214(5):782-91.
- Kurtz J. Specific memory within innate immune systems Trends Immunol. 2005;26:186-192.
- Landsman L, Jung S. Lung macrophages serve as obligatory intermediate between blood monocytes and alveolar macrophages. *J Immunol.* 2007;179(6):3488-94.
- Lavin Y, Winter D, Blecher-Gonen R, David E, Keren-Shaul H, et al. Tissue-resident macrophage enhancer landscapes are shaped by the local microenvironment. *Cell.* 2014;159(6):1312-26.
- Lehnert B. Pulmonary and thoracic macrophage subpopulations and clearance of particles from the lung. *Environ. Health Perspect.* 1992;97:17-46.
- Li F, Piattini F, Pohlmeier L, Feng Q, Rehrauer H, et al. Monocyte-derived alveolar macrophages autonomously determine severe outcome of respiratory viral infection. *Sci Immunol.* 2022;7(73):eabj5761.
- Liew P, Kubes P. The Neutrophil's Role During Health and Disease. *Physiol Rev.* 2019;99(2):1223-1248.
- Lighthart, B. Mini-review of the concentration variations found in the alfresco atmospheric bacterial populations. *Aerobiologia* 2000;16:7-16.
- Liu Z, Gu Y, Chakarov S, Bleriot C, Kwok I, et al. Fate Mapping via Ms4a3-Expression History Traces Monocyte-Derived Cells. *Cell.* 2019;178(6):1509-1525.e19.

- Looney M, Thornton E, Sen D, Lamm W, Glenny R, et al. Stabilized imaging of immune surveillance in the mouse lung. *Nat Methods*. 2011;8(1):91-6.
- Louria D, Blumenfeld H., Ellis E, Kilbourne E, Rogers D. Studies on influenza in the pandemic of 1957–1958. II. Pulmonary complications of influenza. *J Clin Invest*. 1959;38:213–265.
- MacCallum W. Pathological anatomy of pneumonia associated with influenza. *Johns Hopkins Hosp. Rep*. 1921;20:149.
- Machiels B, Dourcy M, Xiao X, Javaux J, Mesnil C, et al. A gammaherpesvirus provides protection against allergic asthma by inducing the replacement of resident alveolar macrophages with regulatory monocytes. *Nat Immunol*. 2017;18(12):1310-1320.
- Madisen L, Zwingman T, Sunkin S, Oh S, Zariwala H, et al. A robust and high-throughput Cre reporting and characterization system for the whole mouse brain. *Nature neuroscience*. 2010;13:133–140
- Mao H, Kano G, Hudson SA, Brummet M, Zimmermann N, et al. Mechanisms of Siglec-F-induced eosinophil apoptosis: a role for caspases but not for SHP-1, Src kinases, NADPH oxidase or reactive oxygen. *PLoS One*. 2013;8(6):e68143.
- Martin F, Parker D, Harfenist B, Soong G, Prince A. Participation of CD11c(+) leukocytes in methicillin-resistant *Staphylococcus aureus* clearance from the lung. *Infect Immun*. 2011;79(5):1898-904.
- Mata E, Tarancon R, Guerrero C, Moreo E, Moreau F, et al. Pulmonary BCG induces lung-resident macrophage activation and confers long-term protection against tuberculosis. *Sci Immunol*. 2021;6(63):eabc2934.
- McQuattie-Pimentel A, Ren Z, Joshi N, Watanabe S, Stoeger T, et al. The lung microenvironment shapes a dysfunctional response of alveolar macrophages in aging. *J Clin Invest*. 2021;131(4):e140299.
- Merad M, Manz M, Karsunky H, Wagers A, Peters W, et al. Langerhans cells renew in the skin throughout life under steady-state conditions. *Nat Immunol*. 2002;3(12):1135-41.
- Miles P, Wright J, Bowman L, Castranova V. Incorporation of (3H)palmitic acid into disaturated phosphatidylcholine in alveolar type II cells isolated by centrifugal elutriation. *Biochim. Biophys. Acta*. 1983;753:107-118.
- Misharin A, Morales-Nebreda L, Reyfman P, Cuda C, Walter J, et al. Monocyte-derived alveolar macrophages drive lung fibrosis and persist in the lung over the life span. *J Exp Med*. 2017;214(8):2387-2404.
- Mitroulis I, Ruppova K, Wang B, Chen LS, Grzybek M, et al. Modulation of Myelopoiesis Progenitors Is an Integral Component of Trained Immunity. *Cell*. 2018;172(1-2):147-161.e12.

Moorlag S, Khan N, Novakovic B, Kaufmann E, Jansen T, et al. β -Glucan Induces Protective Trained Immunity against Mycobacterium tuberculosis Infection: A Key Role for IL-1. *Cell Rep.* 2020;31(7):107634.

Morris D, Huang X, Kaminski N, Wang Y, Shapiro SD, et al. Loss of integrin α (v) β 6-mediated TGF- β activation causes Mmp12-dependent emphysema. *Nature.* 2003;422(6928):169-73.

Mould K, Barthel L, Mohning M, Thomas S, McCubbrey A, et al. Cell Origin Dictates Programming of Resident versus Recruited Macrophages during Acute Lung Injury. *Am J Respir Cell Mol Biol.* 2017;57(3):294-306.

Nakata K, Gotoh H, Watanabe J, Uetake T, Komuro I, et al. Augmented proliferation of human alveolar macrophages after allogeneic bone marrow transplantation. *Blood.* 1999;93(2):667-73.

Netea M, Joosten L, Latz E, Mills K, Natoli G, et al. Trained immunity: A program of innate immune memory in health and disease. *Science.* 2016;352(6284):aaf1098.

Netea M, Domínguez-Andrés J, Barreiro L, Chavakis T, Divangahi M, et al. Defining trained immunity and its role in health and disease. *Nat Rev Immunol.* 2020;20(6):375-388.

Neupane A, Willson M, Chojnacki A, Vargas E Silva Castanheira F, et al. Patrolling Alveolar Macrophages Conceal Bacteria from the Immune System to Maintain Homeostasis. *Cell.* 2020;183(1):110-125.e11.

Noble P, Henson C. Lucas M, Mora-Worms P, et al. "Transforming growth factor- β primes macrophages to express inflammatory gene products in response to particulate stimuli by an autocrine/paracrine mechanism." *Journal of Immunology.* 1993;151(2):979-89.

Opie E, Blake F, Small J, Rivers T. Epidemic Respiratory Disease: The Pneumonias and Other Infections of the Respiratory Tract Accompanying Influenza and Measles. St. Louis: C.V. Mosby Co.; 1921.

Ostuni R, Piccolo V, Barozzi I, Polletti S, Termanini A, et al. Latent enhancers activated by stimulation in differentiated cells. *Cell.* 2013;152(1-2):157-71.

Palecanda A, Paulauskis J, Al-Mutairi E, Imrich A, Qin G, et al. Role of the scavenger receptor MARCO in alveolar macrophage binding of unopsonized environmental particles. *J Exp Med.* 1999;189(9):1497-506.

Palucka A, Banchereau J. Langerhans cells: daughters of monocytes. *Nat Immunol.* 2006;7:223–224.

Passlick B, Flieger D, Ziegler-Heitbrock H. Identification and characterization of a novel monocyte subpopulation in human peripheral blood. *Blood.* 1984;74(7):2527-34.

Pastuszka J, Paw U, Lis D, Wlazło K, et al. Bacterial and fungal aerosol in indoor environment in Upper Silesia. *Atmos. Environ.* 2000;34:3833-3842.

Peão M, Aguas A, de Sá C, Grande N. Morphological evidence for migration of particle-laden macrophages through the interalveolar pores of Kohn in the murine lung. *Acta Anat.* 1993;147:227-232.

Peters W, Scott H, Chambers H, Flynn J, Charo I, et al. Chemokine receptor 2 serves an early and essential role in resistance to *Mycobacterium tuberculosis*. *Proc. Natl. Acad. Sci.* 2001;98:7958-7963.

Purnama C, Ng S, Tetlak P, Setiagani Y, Kandasamy M, et al. Transient ablation of alveolar macrophages leads to massive pathology of influenza infection without affecting cellular adaptive immunity. *Eur J Immunol.* 2014;44(7):2003-12.

Quintin J, Saeed S, Martens J, Giamarellos-Bourboulis E, Ifrim D, et al. *Candida albicans* infection affords protection against re-infection via functional reprogramming of monocytes. *Cell Host Microbe.* 2012;12(2):223-32.

Rasmussen L, Lipsky P, Seljelid R. Production of prostaglandin E2 and interleukin 1 by mouse peritoneal macrophages stimulated with beta-1,3-D-glucan derivatized plastic beads. *Scand J Immunol.* 1987;(6):731-6.

Reynolds J, Kastello M, Harrington D, Crabbs C, Peters C.J et al. Glucan-induced enhancement of host resistance to selected infectious diseases. *Infect. Immun.* 1980;30(1):51-57.

Roquilly A, Jacqueline C, Davieau M, Mollé A, Sadek A, et al. Alveolar macrophages are epigenetically altered after inflammation, leading to long-term lung immunoparalysis. *Nat Immunol.* 2020;21(6):636-648.

Rubin-Bejerano I, Abeijon C, Magnelli P, Grisafi P, Fink GR. Phagocytosis by human neutrophils is stimulated by a unique fungal cell wall component. *Cell Host Microbe.* 2007 Jul 12;2(1):55-67.

Russell CA, Jones TC, Barr IG, et al. The global circulation of seasonal influenza A (H3N2) viruses. *Science.* 2008;320:340-6

Sanders C, Vogel P, McClaren J, Bajracharya R, Doherty P, et al. Compromised respiratory function in lethal influenza infection is characterized by the depletion of type I alveolar epithelial cells beyond threshold levels. *Am J Physiol Lung Cell Mol Physiol.* 2013;304(7):L481-8.

Schmit T, Guo K, Tripathi J, Wang Z, McGregor B, et al. Interferon- γ promotes monocyte-mediated lung injury during influenza infection. *Cell Rep.* 2022;38(9):110456.

Schneider C, Nobs S, Heer A, Kurrer M, Klinke G, et al. Alveolar macrophages are essential for protection from respiratory failure and associated morbidity following influenza virus infection. *PLoS Pathog.* 2014;10(4):e1004053.

Schulz C, Gomez Perdiguero E, Chorro L, Szabo-Rogers H, Cagnard N, et al. A lineage of myeloid cells independent of Myb and hematopoietic stem cells. *Science.* 2012;336:86–90.

Scott C, Zheng F, De Baetselier P. et al. Bone marrow-derived monocytes give rise to self-renewing and fully differentiated Kupffer cells. *Nat Commun* 2016;7:10321.

Scott C, Henri S, and Guilliams M. Mononuclear phagocytes of the intestine, the skin, and the lung. *Immunol. Rev.* 2014;262:9–24.

Serbina N, Jia T, Hohl T, Pamer E. Monocyte-mediated defense against microbial pathogens. *Annu Rev Immunol.* 2008;26:421-52.

Somerville L, Cardani A, Braciale T. Alveolar Macrophages in Influenza A Infection Guarding the Castle with Sleeping Dragons. *Infect Dis Ther.* 2020;1(1):10.31038.

Subramanian S, Busch C, Molawi K. et al. Long-term culture-expanded alveolar macrophages restore their full epigenetic identity after transfer in vivo. *Nat Immunol.* 2022;23:458–468.

Summary of the 2011-2012 Influenza Season. WHO. 2012.
<https://www.cdc.gov/flu/pastseasons/1112season.htm>

Surewaard B, Deniset J, Zemp F, Amrein M, Otto M, et al. Identification and treatment of the *Staphylococcus aureus* reservoir in vivo. *J Exp Med.* 2016;213(7):1141-51.

Sun K, Metzger DW. Inhibition of pulmonary antibacterial defense by interferon-gamma during recovery from influenza infection. *Nat Med.* 2008;14(5):558-64.

Takahashi K, Yamamura F, Naito M. Differentiation, maturation, and proliferation of macrophages in the mouse yolk-sac: a light-microscopic, enzyme-cytochemical, immunohistochemical, and ultrastructural study. *J. Leukoc. Biol.* 1989;45:87–96.

Takeda K, Clausen B, Kaisho T, Tsujimura T, Terada N, et al. Enhanced Th1 activity and development of chronic enterocolitis in mice devoid of Stat3 in macrophages and neutrophils. *Immunity.* 1999;10(1):39-49.

Takeya M. and Takahashi K. Ontogenic development of macrophage subpopulations and Ia-positive dendritic cells in fetal and neonatal rat spleen. *J. Leukoc. Biol.* 1992;52, 516-523.

Tarling J, Lin H, Hsu S. Self-renewal of pulmonary alveolar macrophages -evidence from radiation chimera studies. *J Leukoc Biol.* 1987;42(5):443–446.

- Thanabalasuriar A, Kubes P. Patrolling Alveolar Macrophages Conceal Bacteria from the Immune System to Maintain Homeostasis. *Cell*. 2020;183(1):110-125.e11..
- Tribouley J, Tribouley-Duret J, Appriou M. Effect of Bacillus Callmette Guerin (BCG) on the receptivity of nude mice to *Schistosoma mansoni*. *C. R. Seances Soc. Biol. Fil.* 1978;172, 902–904.
- Tsou C, Peters W, Si Y, Slaymaker S, Aslanian AM, et al. Critical roles for CCR2 and MCP-3 in monocyte mobilization from bone marrow and recruitment to inflammatory sites. *J Clin Invest*. 2007;117(4):902-9.
- Tsuboi N. et al. Roles of Toll-like receptors in C-C chemokine production by renal tubular epithelial cells. *J. Immunol.* 2002;169, 2026–2033.
- van de Laar L, Saelens W, De Prijck S, Martens L, Scott CL, et al. Yolk-sac Macrophages, Fetal Liver, and Adult Monocytes Can Colonize an Empty Niche and Develop into Functional Tissue-Resident Macrophages. *Immunity*. 2016;44(4):755-68.
- van Furth R, Cohn ZA. The origin and kinetics of mononuclear phagocytes. *J Exp Med*. 1968;128(3):415-35.
- van oud Alblas A, van Furth R. Origin, Kinetics, and characteristics of pulmonary macrophages in the normal steady state. *J Exp Med*. 1979;149(6):1504-18.
- van 't Wout J, Poell R, van Furth R. The role of BCG/PPD-activated macrophages in resistance against systemic candidiasis in mice. *Scand J Immunol*. 1992;36(5):713-9.
- Veldhuizen E, Waring A, Walther F, Batenburg J, van Golde L et al. Dimeric N-terminal segment of surfactant protein B (dSP-B1–25) has enhanced surface properties compared to monomeric SP-B1–25 *Biophys. J.* 2000;79:pp. 377-384.
- Virolainen M. Hematopoietic origin of macrophages as studied by chromosome markers in mice. *J Exp Med*. 1968 May 1;127(5):943-52.
- Wang J, Kubes P. A Reservoir of Mature Cavity Macrophages that Can Rapidly Invade Visceral Organs to Affect Tissue Repair. *Cell*. 2016;165(3):668-78.
- Wang T, Zhang J, Wang Y, Li Y, Wang L, et al. Influenza-trained mucosal-resident alveolar macrophages confer long-term antitumor immunity in the lungs. *Nat Immunol*. 2023;24(3):423-438.
- Ward H, Nicholas T. Alveolar type I and type II cells. *Aust N Z J Med*. 1984;14(5 Suppl 3):731-4.
- Wertheim H, Melles D, Vos M, van Leeuwen W, van Belkum A, et al. The role of nasal carriage in *Staphylococcus aureus* infections. *Lancet Infect Dis*. 2005;5(12):751-62.

- Westphalen K, Gusarova G, Islam M, Subramanian M, Cohen TS, et al. Sessile alveolar macrophages communicate with alveolar epithelium to modulate immunity. *Nature*. 2014;506(7489):503-6.
- Yajjala V, Thomas V, Bauer C, Scherr T, Fischer K, et al. Resistance to Acute Macrophage Killing Promotes Airway Fitness of Prevalent Community-Acquired Staphylococcus aureus Strains. *J Immunol*. 2016;196(10):4196-203.
- Yáñez A, Coetzee S, Olsson A, Muench D, Berman B, et al. Granulocyte-Monocyte Progenitors and Monocyte-Dendritic Cell Progenitors Independently Produce Functionally Distinct Monocytes. *Immunity*. 2017;47(5):890-902.e4.
- Yao Y, Jeyanathan M, Haddadi S, Barra NG, Vaseghi-Shanjani M, et al. Induction of Autonomous Memory Alveolar Macrophages Requires T-cell Help and Is Critical to Trained Immunity. 2018;175(6):1634-1650.e17.
- Yipp B, Kim J, Lima R, Zbytnuik L, Petri B, et al. The Lung is a Host Defense Niche for Immediate Neutrophil-Mediated Vascular Protection. *Sci Immunol*. 2017;28;2(10):eaam8929.
- Yona S, Kim K, Wolf Y, Mildner A, Varol D, et al. Fate mapping reveals origins and dynamics of monocytes and tissue macrophages under homeostasis. *Immunity*. 2013;38(1):79-91.
- Yoshimura A, Naka T, Kubo M. SOCS proteins, cytokine signalling and immune regulation. *Nat Rev Immunol*. 2007;7:454-65.
- Young S, Ye J, Frazer DG, Shi X, Castranova V. Molecular mechanism of tumor necrosis factor- α production in 1 \rightarrow 3-beta-glucan (zymosan)-activated macrophages. *J Biol Chem*. 2001;8;276(23):20781-7.
- Yun C, Estrada A, Van Kessel A, Gajadhar A, Redmond M et al. Beta-(1 \rightarrow 3, 1 \rightarrow 4) oat glucan enhances resistance to *Eimeria vermiformis* infection in immunosuppressed mice. *Int. J. Parasitol*. 1997;27(3):329-337.
- Zasłona Z, Przybranowski S, Wilke C, van Rooijen N, Teitz-Tennenbaum et al. Resident alveolar macrophages suppress, whereas recruited monocytes promote, allergic lung inflammation in murine models of asthma. *J Immunol*. 2014;193(8):4245-53.
- Zaynagetdinov R, Sherrill T, Kendall P, Segal B, Weller KP, et al. Identification of myeloid cell subsets in murine lungs using flow cytometry. *Am J Respir Cell Mol Biol*. 2013;49(2):180-9.
- Zhang M, Angata T, Cho J, Miller M, Broide DH, et al. Defining the in vivo function of Siglec-F, a CD33-related Siglec expressed on mouse eosinophils. *Blood*. 2007;109(10):4280-7.
- Zhu Y, Thomas G, Hedrick C, Jeffrey M. Hoeg Award Lecture: Transcriptional Control of Monocyte Development. *Arterioscler Thromb Vasc Biol*. 2016;36:1722-1733.

Appendix A

Table 1. List of antibodies used

Antibody	Source
PerCP-Cy5.5 Anti-Mouse CD11c (Clone: N418)	Biolegend Catalog number: 117326
SuperBright 780 Anti-Mouse CD11c (Clone: N418)	ThermoFisher Scientific Catalog number: 78-0114-82
FITC Anti-Mouse CD11b (Clone: M1/70)	ThermoFisher Scientific Catalog number: 11-0112-82
PE-Cy7 Anti-Mouse CD11b (Clone: M1/70)	ThermoFisher Scientific Catalog number: 25-0112-82
BV510 Anti-Mouse CD45 (Clone: 30-F11)	Biolegend Catalog number: 103137
APC-Cy7 Anti-Mouse Ly6G (Clone: 1A8)	Biolegend Catalog number: 127624
PacBlue Anti-Mouse Ly6G (Clone: 1A8)	Biolegend Catalog number: 127612
PE Anti-Mouse SiglecF (Clone: E50-2440)	BD BioScience Catalog number: 562068
AF647 Anti-Mouse SiglecF (Clone: E50-2440)	BD BioScience Catalog number: 562680
APC-Cy7 Anti-Mouse MHCII (Clone: M/5114.15.2)	Biolegend Catalog number: 107628
AF647 Anti-Mouse CD64 (Clone: X54-5/7)	BD BioScience Catalog number: 558539
AF647 Anti-Mouse CD31 (Clone: 390)	Biolegend Catalog number: 102416
Ghost Red Fixable Viability Dye 710	New England Biolabs Catalog number: 90232S
PE-Cy7 Anti-mouse MERTK (Mer) (Clone: 2B10C420)	Biolegend Catalog number: 151521

Table 2. List of bacteria and virus used

Bacterial and viral strains	Source
<i>Staphylococcus aureus</i> (Strain MW2)	Used by Dr. Ajitha Thanabalasuriar.
Influenza A virus (strain A/Puerto Rico/8/1934 H1N1; PR8)	ATCC Catalog number: VR-95

Table 2. List of chemicals, peptides, and reagents used

Reagents	Source
PKH26 Phagocytic Cell Labeling Kit	Sigma Catalog number: PKH26PCL
CellVue® Claret Far Red Fluorescent Cell Dye	Sigma-Aldrich
Chlodronate Liposome	www.clodronateliposomes.org Catalog number: C-005
EDTA (0.5M, pH 8.0)	Ambion

	Catalog number: AM9261
BSA	Sigma Catalog number: A4503
ACK lysis buffer	Gibco Catalog number: A1049201
DNase I	QIAGEN Catalog number: 79254
PFA (16% Solution)	EMS Catalog number: 15710
DMEM	Thermofisher Catalog number: 10313021
MDCK cells	Thermofisher Catalog number: CCL-34
Penicillin/Streptomycin	Thermofisher Catalog number: 15140122
FBS	VWR Catalog number: 97068-088
Trypan blue	Gibco Catalog number: 15250061
2.4% colloidal cellulose	Sigma Catalog number: 9004-34-6
Bovine TPCK trypsin	Thermofisher Catalog number: 20233
2X MEM	Thermofisher Catalog number: 11935046
β -glucan	Sigma Catalog number: G-5011

Table 4. List of software used

Software	Source
FlowJo Software	TreeStar www.flowjo.com
Imaris	Oxford instruments www.imaris.oxinst.com/
GraphPad Prism v8 software	GraphPad
BioRender	BioRender